Appendix A: Geometric and electronic properties in a series of phosphorescent heteroleptic Cu(I) complexes: Crystallographic and computational studies

Katharina Kubiček[a,b,*], Sreevidya Thekku Veedu[a,b], Darina Storozhuk[a,b,c], Reza Kia[a,b,1,*], and Simone Techert[a,b,c,*]

[a]*FS-SCS, Deutsches Elektronen-Synchrotron (DESY), Notkestraße 85, 22607 Hamburg, Germany*

[b]*Max Planck Institute for Biophysical Chemistry, Am Fassberg 11, 37077 Göttingen, Germany*

[c]*Institute of X-ray Physics, Georg-August-Universität Göttingen, Friedrich-Hund-Platz 1, 37077 Göttingen, Germany*

[*]Corresponding authors. *E-mail addresses*: katharina.kubicek@desy.de (K.K.); rkia@sharif.edu (R.K.); simone.techert@desy.de (S.T.).

[1]Present address: Chemistry Department, Sharif University of Technology, P.O. Box 11155-3516, Tehran, Iran

Supplementary materials:

A1. Synthesis and chemical analysis of the Cu(I) complexes

A1.1. Synthesis

*A1.1.1. [Cu(phen)(DPEphos)]BF_4 (**1**).*

A mixture of Tetrakis(acetonitrile)copper(I) tetrafluoroborate ($[Cu(NCCH_3)_4]BF_4$, 3.11 g, 33.0 mmol) and Bis[(2-diphenylphosphino)phenyl]ether ($O[C_6H_4P(C_6H_5)_2]_2$, DPEphos, 5.33 g, 33.0 mmol) in 300 ml of CH_2Cl_2 was stirred at room temperature for 3 h. Upon addition of 1,10-Phenanthroline ($C_{12}H_8N_2$, phen, 1.78 g, 33.0 mmol) the clear solution turned bright yellow, remained clear, and was stirred for an additional 2 h. Approximately 900 ml of diethyl ether ($(CH_3CH_2)_2O$) was added to the solution to precipitate a bright yellow solid. The solution containing the newly precipitated solid was then left in the refrigerator for one day. It was vacuum filtered using a medium frit, washed with diethyl ether and dried under vacuum. A bright yellow powder was isolated (yield: 8.00 g, 93 %). Analysis: ESI-MS (*m/z*) = 781 ($[Cu(phen)(DPEphos)]^+$). IR (cm^{-1}): 3056w, 1587w, 1568w, 1510w, 1480w, 1463m, 1436s, 1261m, 1216m, 1184w, 1161w, 1142w, 1096s, 1058vs, 998w, 848m, 803w, 748m, 728m, 697m. ^1H NMR (400MHz, CD_3CN, r.t.): δ 8.83 (2H, d, J= 4.6 Hz), 8.57 (2H, d, J = 8.3 Hz), 8.09 (2H, s), 7.70 (2H, dd, J= 4.8 Hz, J = 8.1 Hz), 7.43-7.36 (2H, m), 7.34-7.26 (4H, t, J = 7.4 Hz), 7.20-7.11 (10H, t, J = 7.4 Hz), 7.09-7.00 (10H, m), 6.81-6.72 (2H, m).

For the synthesis of compounds **2** and **6** essentially identical procedures to that described for compound **1** were used. Only the quantities for additional starting materials and product yields are given.

*A1.1.2. [Cu(dmp)(DPEphos)]BF_4 (**2**).*

2,9-Dimethyl-1,10-phenanthroline ($C_{14}H_{12}N_2$, 2.06 g, 33.0 mmol). A neon yellow powder was isolated (yield: 7.28 g, 82 %). Analysis: ESI-MS (*m/z*) = 810 ($[Cu(dmp)(DPEphos)]^+$). IR (cm^{-1}): 3056w, 1593w, 1564w, 1504w, 1480w, 1462m, 1436s, 1261w, 1223m, 1157w, 1096s, 1057vs, 998w, 859w, 802w, 748m, 698m. ^1H NMR (400MHz, CD_3CN, r.t.): δ 8.41 (2H, d, J = 7.8 Hz), 7.91 (2H, s), 7.61 (2H, d, J = 7.4 Hz), 7.46-7.38 (2H, m), 7.35-7.18 (8H, m), 7.10-6.96 (18H, m), 2.45 (6H, s).

*A1.1.3. [Cu(bq)(DPEphos)]PF_6 (**6**).*

Tetrakis(acetonitrile)copper(I) hexafluorophosphate ($[Cu(NCCH_3)_4]PF_6$, 3.69 g, 33.0 mmol). 2,2'-Biquinoline ($C_{18}H_{12}N_2$, 2.54 g, 33.0 mmol). A bright orange powder was isolated (yield: 7.94 g, 80 %). Analysis: ESI-MS (*m/z*) = 857 ($[Cu(bq)(DPEphos)]^+$). IR (cm^{-1}): 3056w, 1593w, 1507w,1463w, 1436m, 1261w, 1220m, 1096w, 876m, 839vs, 784w, 746m, 697m. ^1H NMR (400MHz, CD_3CN, r.t.): δ 8.58 (2H, s), 8.32 (2H, s), 8.01 (2H, d, J = 8.2 Hz), 7.71-6.58 (32H, m).

A1.2. Analysis of the synthesis products

Mass spectra of the compounds were recorded on a Varian MS-500, Electrospray Ionization Mass Spectrometer (ESI-MS). The experimental and simulated spectra are displayed in Fig. A1. The molecular ion peaks observed in the ESI-MS are in agreement with the cationic structures shown in Fig. 1 in the main article.

A Bruker IFD 25 FT-IR spectrophotometer was used to record infrared spectra of the complexes in KBr pellets in the region from 4000 cm^{-1} to 600 cm^{-1} (Figs. A2-A4). The spectra displayed a

very strong band at ~ 1058 cm^{-1} for **1** and **2** and at ~ 839 cm^{-1} for **6** which can be assigned to the BF_4^- and PF_6^- anion respectively.

^1H NMR spectra were obtained by an Agilent Oxford 400 MHz spectrometer with tetramethylsilane (TMS) as an internal standard. The compounds were dissolved in deuterated acetonitrile (CD_3CN). In agreement with previous reports for the compounds [4,5] the DPEphos and phen/bq ligand protons appear as ^1H NMR signal including complex sets of overlapping multiplets with chemical shifts (ppm) of + 8.83 to + 6.76 (Figs. A5-A7). For complex **1** the two protons of the phen ligand at the position of the methyl groups in complex **2** are associated with a doublet with a center at + 8.83. The methyl proton resonances of complex **2** can be found at + 2.45. For all NMR spectra peaks located at + 5.47, + 2.14, + 1.96 and + 1.44 are caused by residual solution dichloromethane (DCM), methanol, acetonitrile (ACN) and diethyl ether respectively.

A2. Molecular ground state structures: X-ray crystallography and density functional theory (DFT)

A2.1. Integration and refinement of the X-ray crystallography data

The X-ray diffraction (XRD) data were indexed and integrated with the program package APEX2 [7]. Multi-scan absorption corrections were applied by using the SCALE program [7] for area detector. The crystal structure was solved and refined with SHELXTL program package [8]. All of the non-hydrogens are refined anisotropically and hydrogen atoms on carbons were placed in idealized positions (C-H = 0.93 or 0.96 Å) and included as riding with Uiso(H) = 1.2 or 1.5 Ueq(non-H). For molecular graphics the program SHELXTL, OLEX [9] and MERCURY [10] were used. All calculations were carried out using the PLATON software [11].

A2.2. Comaprison of structures

Two different structures of the same complex were compared quantitatively at a time. Since positions of light elements are more difficult to determine from X-ray diffraction due to the dependency of the scattering amplitude on the nuclear charge, we have excluded hydrogen atoms in the present analysis. Following the approach described by Minenkov et al. [12], to investigate deviations between geometries for two structures, the mean signed error (MSE) and mean unsigned error (MUE) for the difference in all their interatomic distances and in bonding distances to the Cu(I) coordination center respectively were evaluated. The MSE and MUE were calculated according to MSE = 2/(N(N-1))*Σ_i^N-1Σ_j>i^N (|Rij(DFT)-Rij(X-ray)|) MUE = 2/(N(N-1))*Σ_i^N-1Σ_j>i^N (Rij(DFT)-Rij(X-ray)) [12]. Here, Rij is the interatomic distance between atom i and j and N is the number of atoms. Such an interatomic distances approach allows to study systematic variations in bond lengths that are not easy to access by a simple comparison of molecular Cartesian coordinates [12]. Moreover, due to the fact that errors in Rij(DFT)-Rij(X-ray) are larger for larger |Rij(DFT)-Rij(X-ray)|, large distances dominate the MSE and MUE for complexes **1**-**6**. Such large distances are influenced by Van der Waals interactions. The all distances approach therefore allows to test the ability of density functionals to describe those interactions. It should be noted that uncertainties from vibrational effects due to the finite temperature during our XRD measurement were considered small in comparison to deviations of results between functionals, and therefore are not included in the present analysis.

A2.3. Comparison of our crystal structures with previous X-ray crystallography results [1-6]

In Tab. A1 we compare important bond lengths (Å) and angles (deg) of the complexes in their ground state in single crystals as derived in this work (Exp.) and by Kuang et al. [2] and Zhang et

al. [5]. Results in [1,3,4] and [6] are similar to [2] and our results respectively and thus omitted here.

In contrast to former studies where complex **1** crystallized in a triclinic P-1 space group with $[Cu(phen)(DPEphos)]BF_4 \cdot 1.5EtO_2 \cdot CH_3CN$ composition [1-4], analogue to Ref. [6], we observed a monoclinic crystal system with $P2_1/n$ symmetry. However, in contrast to Costa et al. [6] who report a $[Cu(phen)(DPEphos)]PF_6 \cdot CH_2Cl_2$ composition, we found a $[Cu(phen)(DPEphos)]BF_4 \cdot CH_3OH \cdot 0.36 \cdot H_2O$ structure and a disorder of the phen ligand (two positions with occupancy of 75:25) and the BF_4^- counterion (86:14) for the asymmetric unit. For complex **6**, instead of a monoclinic crystal system with $P2_1/n$ symmetry and $[Cu(bq)(DPEphos)]BF_4 \cdot 2 \cdot CH_3O$ composition, we measured a triclinic P-1 space group with $[Cu(bq)(DPEphos)]PF_6 \cdot 0.5 \cdot CH_2Cl_2 \cdot 0.2\ H_2O$ structure and partially occupied DCM (50%) and water (20%) for the asymmetric unit [5]. Only for complex **2** the system crystallized in the same monoclinic $P2_1/c$ space group as previously reported [1-4], but in contrast to a $[Cu(dmp)(DPEphos)]BF_4 \cdot CH_2Cl_2$ structure, we observed a $[Cu(dmp)(DPEphos)]BF_4 \cdot CH_3CN$ composition. In all our crystals no significant intermolecular interactions are found.

In Fig. A8 we superpose the molecular structures of complex **2** and **6** respectively as determined by XRD within this work and by Kuang et al. [2] and by Zhang et al. [5]. A comparison for complex **1** can be found in the main article, Fig. 2.

A2.4. Comparison of DFT calculated and XRD molecular structures

In Fig. A9-A14 we superpose molecular structures of complexes **1-6** as calculated by DFT and measured in different XRD experiments.

A3. Molecular orbitals, electronic structure of the ground state

A3.1. Electronic structures: Density functional validation studies

Electronic structures, and in particular HOMO-LUMO gap energies, are very sensitive to the applied functional [13]. We have evaluated the HOMO-LUMO gap energies for calculations with seven different functionals (main article) and the results are shown in Tab. 2. Distinct "absorption edges" are observed in our UV-VIS spectra of the complexes in solution (Fig. A 19) and in previous reports of such spectra [15,14,15]. All absorption occurs at energies higher than that of the absorption edge energy. In general, non-hybrid functionals (PBE [16], B97D3 [17], M06L [18,19]) predict HOMO-LUMO energy gaps which are significantly lower in energy than the corresponding measured absorption edges. On the other hand the ωB97XD functional [20,21] which includes additional long-range corrections gives dramatically higher energy gaps than expected from the absorption spectra of the complexes. The hybrid functionals B3LYP [22,23], PBE0-GD3 [24-26] and M06 [18,19] can reproduce measured absorption spectra most accurately.

A3.2. Molecular orbital energies and partial density of states

In Tab. A3-8 we list molecular orbital energies and percentage compositions of selected frontier molecular orbitals (MOs) expressed in terms of component fragments for the ground state of complexes **1-6** in DCM as calculated by DFT (G09, [28]) at the PBE0-GD3 level [24-26]. Graphic presentations of the results for DCM are depicted in the Figs. 5 (main article) and A15-A17.

A4. Ground state absorption

A4.1. Experimental absorption and emission spectra

Electronic absorption and emission spectra for compounds **1, 2** and **6** in DCM and ACN solution were measured in the region from 320-800 nm and 500-800 nm respectively (Fig. A19). As observed in previous work [1-3] the absorption spectra basically consist of two bands: a first band at around 400 nm (~ 3000 M^{-1} cm^{-1}) for complex **1** and **2** and 450 nm (~ 3000 M^{-1} cm^{-1}) for complex **6** respectively and a second intenser band at shorter wavelengths. By comparison with absorption spectra of homoleptic Cu(I) compounds the former has been attributed to a CT transition while the latter has been assigned to ligand-centered (LC) transitions. A comparison of complex **1, 2** and **6** in DCM shows that the first absorption maximum for complex **1** is about ~10 nm shifted (392 nm) compared to complex **2** (382 nm) and the first absorption maximum for complex **6** is even more red-shifted, by around 70 nm (449 nm). In the more polar solvent ACN the first absorption band of all three compounds experiences a blue-shift which is ~ 8 nm (384 nm) for complex **1** and ~7nm for complex **2** (375 nm) and complex **6** (442 nm) respectively. For all compounds emission maxima are red-shifted with respect to their respective absorption maxima and complex **1** and **6** exhibit a larger shift than complex **2**. Moreover, emission spectra show similar emission yields for complex **1** and **6** but in contrast, complex **2** exhibits a two orders of magnitude higher emission yield. The reason for both findings is attributed to the geometric torsional relaxation in the excited states of Cu(I) coordination compounds upon promotion of a HOMO electron which is discussed to facilitate formation of pentacoordinated solvent complexes in polar solvents and to compress the energy separation between the ground and excited states and thus to promote non-radiative relaxation [27]. Active ligands are believed

to hamper this torsional relaxation in the excited states and compound **2** has two sterically active methyl groups in its prominent 2,9-positions of the phen unit [27].

A4.2. Absorption spectra: Experiment and DFT

In Fig. 6 (main article) and Fig. A20-A22 we compare experimentally measured and DFT calculated (G09, [28]; PBE0-GD3 [24-26]) ground state absorption spectra for complexes **1-6** in DCM.

A4.3. Triplet excitations

In Tab. A9 we list excitation wavelengths, oscillator strengths and composition of the first two TD-DFT calculated (G09, [28]; PBE0-GD3 [24-26]) lowest triplet excitations for the ground state of the cations of complexes **1-6** in DCM.

A5. Lowest triplet excited state

A5.1. Comparison of the relaxed singlet and the lowest triplet excited state structure

In Fig. A23 we compare the molecular structure of complex **2** in the lowest lying triplet excited state and in the singlet excited state after geometric relaxation as calculated by (TD)-DFT (G09, [28]). Molecular geometries are nearly identical for the two states.

A5.2. Electronic structure of the lowest triplet excited state

In Tab. A10-15 we list molecular orbital energies and percentage compositions of selected frontier MOs expressed in terms of component fragments for the lowest excited triplet state of complexes **1-6** in DCM as calculated by DFT (G09, [28]) at the PBE0-GD3 level [24-26].

References

[1] Cuttell, D.G.; Kuang, S.-M.; Fanwick, P.E.; McMillin, D.R.; Walton, R.A. *J. Am. Chem. Soc.* **2002**, *124*, 6-7.

[2] Kuang, S.-M.; Cuttell, D.G.; McMillin, D.R.; Fanwick, P.E.; Walton, R.A. *Inorg. Chem.* **2002**, *41*, 3313-3322.

[3] Yang, L.; Feng, J.-K.; Ren, A.-M.; Zhang, M.; Ma, Y.-G.; Liu, X.-D. *Eur. J. Inorg. Chem.* **2005**, 1867-1879.

[4] Zhang, K.; Zhang, D. *Spec. Acta Part A* **2014**, *124*, 341-348.

[5] Zhang, Q.; Ding, J.; Cheng, Y.; Wang, L.; Xie, Z.; Jing, X.; Wang, F. *Adv. Funct. Mater.* **2007**, *17*, 2983-2990.

[6] Costa, R. D.; Tordera, D.; Ortí, E.; Bolink, H. J.; Schönle, J.; Graber, S.; Housecroft, C. E.; Constable, E. C.; Zampese, J. A. *J. Mater. Chem.* **2011**, *21*, 16108–16118.

[7] APEX2 (version 2009.11-0). *Program for Bruker CCD X-ray Diffractometer Control*, Bruker AXS Inc., Madison, WI, 2009.

[8] Sheldrick, G.M. *Acta Crystallogr.* **2008**, *A64*, 112−122.

[9] Dolomanov, O.V.; Bourhis, L.J.; Gildea, R.J.; Howard, J.A.K.; and Puschmann, H. *J. Appl. Cryst.* **2009**, *42*, 339-341.

[10] Macrae, C.F.; Edgington, P.R.; McCabe, P.; Pidcock, E.; Shields, G.P.; Taylor, R.; Towler, M.; van de Streek, J. *J. Appl. Cryst.* **2006**, *39*, 453-457.

[11] Spek, A.L. *Acta Crystallogr.* **2009**, *D65*, 148−155.

[12] Minenkov, Y.; Singstad, A.; Occhipinti, G.; Jensen, V.R. *Dalton Trans.* **2012**, *41*, 5526–5541.

[13] Kreutzer, J.; Blaha, P.; Schubert, U. *Comput. Theor. Chem.* **2016**, *1084*, 162-168.

[14] Armaroli, N; Accorsi, G.; Holler, M.; Moudam, O.; Nierengarten, J.F.; Zhou, Z.; Wegh, R.T.; Welter, R. *Adv. Mater.* **2006**, *18*, 1313–1316.

[15] Yao, X.-X.; Guo, Y.-M.; Liu, R.; Feng, X.-Y.; Li, H.-H.; Liu, N.; Yang, F.-L.; Li, X.-L. *Polyhedron* **2015**, *92*, 84-92.

[16] Perdew, J.P.; Burke, K.; Ernzerhof, M. *Phys. Rev. Lett.* **1996**, *77*, 3865-3868.

[17] Grimme, S.; Ehrlich, S.; Goerigk, L. *J. Comp. Chem*. **2011**, *32*, 1456-1465.

[18] Y. Zhao, Y.; Truhlar, D.G. Theor. Chem. Acc. **2008**, *120*, 215.

[19] Y. Zhao, Y.; Truhlar, D.G. Acc. Chem. Res. **2008**, *41*, 157.

[20] Chai, J.D.; Head-Gordon, M. *Phys. Chem. Chem. Phys.* **2008**, *10*, 6615-6620.

[21] Wu, Q.; Yang, W.T. *J. Chem. Phys.* **2002**, *116*, 515-524.

[22] Becke, A.D. *J. Chem. Phys.* **1993**, *98*, 5648-5652.

[23] Lee, C.; Yang, W.; Parr, R.G. *Phys. Rev. B* **1988**, *37*, 785-789.

[24] Perdew, J.P.; Burke, K.; Ernzerhof, M. *Phys. Rev. Lett.* **1996**, *77*, 3865-3868.

[25] Perdew, J.P.; Burke, K.; Ernzerhof, M. *Phys. Rev. Lett.*, **1997**, *78*, 1396.

[26] Grimme, S.; Antony, J.; Ehrlich, S.; Krieg, H. *J. Chem. Phys.* **2010**, *132*, 154104.

[27] Armaroli, N. *Chem. Soc. Rev.* **2001**, *30*, 113-124.

[28] Gaussian 09, Revision E.01, Frisch, M.J.; Trucks, G.W.; Schlegel, H.B.; Scuseria, G.E.; Robb, M.A.; Cheeseman, J.R.; Scalmani, G.; Barone, V.; Mennucci, B.; Petersson, G.A.; Nakatsuji, H.; Caricato, M.; Li, X.; Hratchian, H.P.; Izmaylov, A.F.; Bloino, J.; Zheng, G.; Sonnenberg, J.L.; Hada, M.; Ehara, M.; Toyota, K.; Fukuda, R.; Hasegawa, J.; Ishida, M.; Nakajima, T.; Honda, Y.; Kitao, O.; Nakai, H.; Vreven, T.; Montgomery Jr., J.A.; Peralta, J.E.;

Ogliaro, F.; Bearpark, M.; Heyd, J.J.; Brothers, E.; Kudin, K.N.; Staroverov, V.N.; Keith, T.; Kobayashi, R.; Normand, J.; Raghavachari, K.; Rendell, A.; Burant, J.C.; Iyengar, S.S.; Tomasi, J.; Cossi, M.; Rega, N.; Millam, J.M.; Klene, M.; Knox, J.E.; Cross, J.B.; Bakken, V.; Adamo, C.; Jaramillo, J.; Gomperts, R.; Stratmann, R.E.; Yazyev, O.; Austin, A.J.; Cammi, R.; Pomelli, C.; Ochterski, J.W.; Martin, R.L.; Morukuma, K.; Zakrzewski, V.G.; Voth, G.A.; Salvador, P.; Dannenberg, J.J.; Dapprich, S.; Daniels, A.D.; Farkas, O.; Foresman, J.B.; Ortiz, J.V.; Cioslowski, J.; Fox, D.J. *Gaussian, Inc.,* Wallingford CT, **2013**.

Tables

Tab. A1. Important bond lengths (Å) and angles (deg) of complexes **1**, **2** and **6** in their ground state in single crystals as derived in this work (Exp.) and by Kuang et al. [2] and Zhang et al. [5]. Note that in the crystallographic data of complex **1** a disordered phen ligand (two positions with occupancy of 75:25) has been refined, hence multiple values for angles and bond lengths are reported.

Complex	**1**		**2**		**6**	
Bond	**Exp.**	**[2]**	**Exp.**	**[2]**	**Exp.**	**[5]**
Cu-N(1)	2.11(1) 2.053(4)	2.071(3)	2.094(2)	2.104(3)	2.087(2)	2.053(4)
Cu-N(2)	2.05(1) 2.078(4)	2.064(3)	2.082(2)	2.084(3)	2.075(2)	2.067(5)
Cu-P(1)	2.1943(8)	2.2314(8)	2.262(7)	2.2691(11)	2.2475(8)	2.3493(19)
Cu-P(2)	2.270(1)	2.2614(9)	2.260(7)	2.2728(11)	2.2535(8)	2.2367(19)
Cu ··O	3.182(2)	3.205	3.153(2)	3.151	3.215(2)	
Angle	**Exp.**	**[2]**	**Exp.**	**[2]**	**Exp.**	**[5]**
N(1)-Cu-N(2)	81.0(5) 81.6(2)	80.83(11)	81.05(8)	80.88(3)	78.93(9)	79.9(2)
N(1)-Cu-P(1)	114.4(3) 123.6(1)	118.37(7)	107.59(6)	107.74(9)	109.15(6)	99.21(14)
N(1)-Cu-P(2)	99.1(3) 103.1(1)	108.11(8)	115.23(6)	115.24(9)	109.35(6)	124.10(15)
N(2)-Cu-P(1)	103.5(4)	109.09(8)	121.56(6)	121.45(9)	117.70(6)	101.83(14)

	100.9(2)					
N(2)-Cu-P(2)	131.5(4)	125.75(8)	110.49(6)	109.98(9)	114.02(6)	123.73(15)
	123.1(2)					
P(1)-Cu-P(2)	117.50(3)	110.81(3)	115.98(3)	116.44(4)	119.60(3)	119.49(7)

Tab. A2. HOMO-LUMO energy gaps (eV) as calculated by DFT using different functionals [16-26] for complexes **1**-**6**. "Exp. onset" defines the low energy onset of the absorption spectrum as measured in this work and in Refs. [2,14,15]. "Exp. maximum" gives the maximum of the measured absorption band as measured in this work and in Refs. [2,14,15].

Functional	**1**	**2**	**3**	**4**	**5**	**6**
PBE [16]	2.07	2.11	2.11	2.22	1.92	1.66
B3LYP [22, 23]	3.63	3.69	3.72	3.76	3.43	3.17
B97D3 [17]	2.13	2.11	2.14	2.23	2.04	1.79
PBE0-GD3 [24-26]	3.97	4.01	4.02	4.1	3.74	3.51
M06L [18,19]	2.22	2.27	2.22	2.22	2.22	1.88
M06 [18,19]	4.09	4.12	4.17	4.17	3.87	3.64
***ω*B97XD [20,21]**	7.33	7.39	7.4	7.48	7.11	6.86
Exp. onset	2.6	2.6	2.7 [2]	2.6 [14]	2.5 [15]	2.1
Exp. maximum	3.2	3.2	3.3 [2]	3.2 [14]	3.2 [15]	2.8

Tab. A3. G09 [28] PBE0-GD3 [24-26] calculated one-electron energy and percentage composition (rounded) of selected frontier MOs expressed in terms of component fragments for the ground state of complex **1** in DCM.

MO	**Energy (eV)**	**Cu**	**phen**	**DPEphos**	**Character**
214(V)	-0.04	1	73	25	phen/DPEphos
213(V)	-0.1	7	11	82	DPEphos
212(V)	-0.16	84	0	16	Cu/DPEphos
211(V)	-0.23	1	3	95	DPEphos
210(V)	-0.32	3	10	86	DPEphos
209(V)	-0.39	2	2	97	DPEphos
208(V)	-0.42	2	2	97	DPEphos
207(V)	-0.59	4	2	94	DPEphos
206(V)	-0.6	4	1	95	DPEphos
205(V)	-0.71	4	1	95	DPEphos
204(V)	-0.9	3	84	13	phen
203(V)	-0.98	1	2	97	DPEphos
202(V)	-1.11	1	2	97	DPEphos
201(V)	-1.14	2	4	95	DPEphos
200(V)	-1.26	2	2	96	DPEphos
199(V)	-2.12	0	100	0	phen
198(V)	**-2.24**	**2**	**96**	**2**	**phen**
197(O)	**-6.21**	**36**	**7**	**57**	**DPEphos/Cu**
196(O)	-6.74	55	18	28	Cu/DPEphos

195(O)	-6.89	55	18	27	Cu/DPEphos
194(O)	-7.07	4	2	94	DPEphos
193(O)	-7.29	2	75	23	phen/DPEphos
192(O)	-7.48	3	2	96	DPEphos
191(O)	-7.52	3	1	95	DPEphos
190(O)	-7.56	3	16	82	DPEphos/phen
189(O)	-7.6	5	16	79	DPEphos/phen
188(O)	-7.67	6	3	91	DPEphos
187(O)	-7.69	19	33	48	DPEphos/phen
186(O)	-7.71	11	18	70	DPEphos/phen
185(O)	-7.77	10	6	84	DPEphos
184(O)	-7.78	18	1	80	DPEphos/Cu
183(O)	-7.87	18	5	76	DPEphos/Cu
182(O)	-7.89	32	16	53	DPEphos/Cu
181(O)	-7.99	51	7	42	Cu/DPEphos
180(O)	-8.02	43	6	51	DPEphos/Cu
179(O)	-8.08	12	3	84	DPEphos

Tab. A4. G09 [28] PBE0-GD3 [24-26] calculated one-electron energy and percentage composition (rounded) of selected frontier MOs expressed in terms of component fragments for the ground state of complex **2** in DCM.

MO	**Energy (eV)**	**Cu**	**dmp**	**DPEphos**	**Character**
222(V)	0	1	84	15	dmp/DPEphos

221(V)	-0.13	6	2	92	DPEphos
220(V)	-0.13	91	0	9	Cu
219(V)	-0.25	1	11	88	DPEphos
218(V)	-0.29	1	2	97	DPEphos
217(V)	-0.36	1	1	98	DPEphos
216(V)	-0.47	2	1	97	DPEphos
215(V)	-0.55	2	2	96	DPEphos
214(V)	-0.62	6	1	93	DPEphos
213(V)	-0.72	4	3	93	DPEphos
212(V)	-0.79	2	84	14	dmp
211(V)	-0.95	1	2	96	DPEphos
210(V)	-1.11	1	2	97	DPEphos
209(V)	-1.14	1	4	95	DPEphos
208(V)	-1.23	1	1	97	DPEphos
207(V)	-2	0	99	1	dmp
206(V)	**-2.17**	**2**	**96**	**2**	**dmp**
205(O)	**-6.18**	**37**	**7**	**56**	**DPEphos/Cu**
204(O)	-6.85	61	24	15	Cu/dmp
203(O)	-6.88	48	11	41	Cu/DPEphos
202(O)	-7.02	6	11	82	DPEphos
201(O)	-7.13	2	78	20	dmp/DPEphos
200(O)	-7.43	5	35	60	DPEphos/dmp
199(O)	-7.45	4	29	67	DPEphos/dmp

198(O)	-7.49	2	3	96	DPEphos
197(O)	-7.56	5	9	86	DPEphos
196(O)	-7.65	3	9	88	DPEphos
195(O)	-7.66	7	10	83	DPEphos
194(O)	-7.68	11	5	84	DPEphos
193(O)	-7.73	7	2	91	DPEphos
192(O)	-7.76	21	2	76	DPEphos/Cu
191(O)	-7.83	39	2	60	DPEphos/Cu
190(O)	-7.85	42	9	49	DPEphos/Cu
189(O)	-7.94	40	4	56	DPEphos/Cu
188(O)	-7.98	39	5	56	DPEphos/Cu
187(O)	-8.09	9	2	89	DPEphos

Tab. A5. G09 [28] PBE0-GD3 [24-26] calculated one-electron energy and percentage composition (rounded) of selected frontier MOs expressed in terms of component fragments for the ground state of complex **3** in DCM.

MO	**Energy (eV)**	**Cu**	**dbp**	**DPEphos**	**Character**
246(V)	0.02	1	82	17	dbp/DPEphos
245(V)	-0.06	96	0	4	Cu
244(V)	-0.13	2	0	98	DPEphos
243(V)	-0.27	2	17	81	DPEphos/dbp
242(V)	-0.37	1	2	97	DPEphos
241(V)	-0.38	1	1	98	DPEphos

240(V)	-0.46	1	2	97	DPEphos
239(V)	-0.57	2	1	97	DPEphos
238(V)	-0.64	5	3	92	DPEphos
237(V)	-0.7	2	19	79	DPEphos/dbp
236(V)	-0.78	3	67	30	dbp/DPEphos
235(V)	-0.93	1	1	98	DPEphos
234(V)	-1.14	2	5	93	DPEphos
233(V)	-1.21	0	1	99	DPEphos
232(V)	-1.25	1	1	97	DPEphos
231(V)	-1.92	0	99	1	dbp
230(V)	**-2.1**	**1**	**96**	**2**	**dbp**
229(O)	**-6.13**	**38**	**8**	**55**	**DPEphos/Cu**
228(O)	-6.85	62	26	11	Cu/dbp
227(O)	-6.93	48	11	41	Cu/DPEphos
226(O)	-7.02	5	15	80	DPEphos/dbp
225(O)	-7.08	1	73	26	dbp/DPEphos
224(O)	-7.36	2	74	24	dbp/DPEphos
223(O)	-7.47	6	1	93	DPEphos
222(O)	-7.52	2	2	96	DPEphos
221(O)	-7.58	8	15	77	DPEphos/dbp
220(O)	-7.64	3	9	88	DPEphos
219(O)	-7.66	6	2	92	DPEphos
218(O)	-7.69	12	4	84	DPEphos

217(O)	-7.71	10	2	88	DPEphos
216(O)	-7.77	26	3	71	DPEphos/Cu
215(O)	-7.81	43	3	54	DPEphos/Cu
214(O)	-7.83	40	8	52	DPEphos/Cu
213(O)	-7.91	40	3	57	DPEphos/Cu
212(O)	-7.94	28	5	68	DPEphos/Cu
211(O)	-8.04	9	6	86	DPEphos

Tab. A6. G09 [28] PBE0-GD3 [24-26] calculated one-electron energy and percentage composition (rounded) of selected frontier MOs expressed in terms of component fragments for the ground state of complex **4** in DCM.

MO	**Energy (eV)**	**Cu**	**dpep**	**DPEphos**	**Character**
274(V)	0.02	37	57	6	dpep/Cu
273(V)	0.01	37	56	7	dpep/Cu
272(V)	-0.08	0	89	10	dpep
271(V)	-0.11	8	25	67	DPEphos/dpep
270(V)	-0.11	9	85	6	dpep
269(V)	-0.14	1	31	68	DPEphos/dpep
268(V)	-0.17	2	90	9	dpep
267(V)	-0.24	6	47	48	DPEphos/dpep
266(V)	-0.41	1	2	96	DPEphos
265(V)	-0.43	2	8	89	DPEphos
264(V)	-0.47	2	4	94	DPEphos

263(V)	-0.54	2	3	95	DPEphos
262(V)	-0.69	2	16	82	DPEphos/dpep
261(V)	-0.7	2	13	85	DPEphos
260(V)	-0.8	2	5	93	DPEphos
259(V)	-0.89	4	61	35	dpep/DPEphos
258(V)	-1.07	3	2	95	DPEphos
257(V)	-1.22	0	1	99	DPEphos
256(V)	-1.32	1	2	97	DPEphos
255(V)	-2	0	99	1	dpep
254(V)	**-2.15**	**2**	**96**	**2**	**dpep**
253(O)	**-6.25**	**36**	**9**	**55**	**Cu/DPEphos**
252(O)	-6.69	40	12	48	Cu/DPEphos
251(O)	-6.76	61	29	9	Cu/dpep
250(O)	-7.04	3	79	17	dpep/DPEphos
249(O)	-7.11	1	81	18	dpep/DPEphos
248(O)	-7.15	6	41	53	DPEphos/dpep
247(O)	-7.21	1	91	9	dpep
246(O)	-7.28	2	72	25	dpep
245(O)	-7.31	0	80	19	dpep/DPEphos
244(O)	-7.41	3	25	73	DPEphos/dpep
243(O)	-7.48	1	12	87	DPEphos
242(O)	-7.51	1	36	62	DPEphos/dpep
241(O)	-7.52	8	36	55	DPEphos/dpep

240(O)	-7.59	6	6	88	DPEphos
239(O)	-7.66	5	4	91	DPEphos
238(O)	-7.67	3	11	86	DPEphos
237(O)	-7.68	21	9	70	DPEphos/Cu
236(O)	-7.76	6	1	93	DPEphos
235(O)	-7.87	65	4	31	Cu/DPEphos
234(O)	-7.89	49	10	41	Cu/DPEphos
233(O)	-7.94	43	8	49	DPEphos/Cu
232(O)	-8.05	10	3	87	DPEphos
231(O)	-8.12	10	3	87	DPEphos

Tab. A7. G09 [28] PBE0-GD3 [24-26] calculated one-electron energy and percentage composition (rounded) of selected frontier MOs expressed in terms of component fragments for the ground state of complex **5** in DCM.

MO	**Energy (eV)**	**Cu**	**dap**	**DPEphos**	**Character**
222(V)	0.19	2	92	7	dap
221(V)	-0.07	6	1	94	DPEphos
220(V)	-0.16	85	1	14	Cu
219(V)	-0.21	2	2	96	DPEphos
218(V)	-0.3	4	4	92	DPEphos
217(V)	-0.37	1	2	97	DPEphos
216(V)	-0.4	2	3	95	DPEphos
215(V)	-0.57	5	4	91	DPEphos

214(V)	-0.59	2	2	96	DPEphos
213(V)	-0.69	4	3	93	DPEphos
212(V)	-0.74	4	79	16	dap
211(V)	-0.97	0	1	99	DPEphos
210(V)	-1.1	1	1	98	DPEphos
209(V)	-1.12	2	2	97	DPEphos
208(V)	-1.24	2	1	97	DPEphos
207(V)	-1.83	0	99	0	dap
206(V)	**-2.15**	**2**	**96**	**2**	dap
205(O)	**-5.89**	**2**	**95**	**3**	dap
204(O)	-6.2	35	10	55	DPEphos/Cu
203(O)	-6.69	58	21	21	Cu/DPEphos
202(O)	-6.84	54	16	30	Cu/DPEphos
201(O)	-7.05	4	1	95	DPEphos
200(O)	-7.37	3	82	15	dap/DPEphos
199(O)	-7.46	4	3	93	DPEphos
198(O)	-7.5	5	1	95	DPEphos
197(O)	-7.53	4	9	87	DPEphos
196(O)	-7.6	4	5	91	DPEphos
195(O)	-7.65	6	1	93	DPEphos
194(O)	-7.66	12	2	86	DPEphos
193(O)	-7.72	10	2	88	DPEphos
192(O)	-7.76	27	1	72	DPEphos/Cu

191(O)	-7.8	42	7	51	DPEphos/Cu
190(O)	-7.85	29	1	70	DPEphos/Cu
189(O)	-7.92	45	6	49	DPEphos/Cu
188(O)	-7.98	32	1	67	DPEphos/Cu
187(O)	-8.05	6	2	92	DPEphos/Cu
186(O)	-8.53	4	92	3	dap

Tab. A8. G09 [28] PBE0-GD3 [24-26] calculated one-electron energy and percentage composition (rounded) of selected frontier MOs expressed in terms of component fragments for the ground state complex **6** in DCM.

MO	**Energy (eV)**	**Cu**	**bq**	**DPEphos**	**Character**
236(V)	0.27	2	86	11	bq
235(V)	-0.02	8	68	24	bq/DPEphos
234(V)	-0.08	87	5	8	Cu
233(V)	-0.16	2	8	90	DPEphos
232(V)	-0.2	2	6	91	DPEphos
231(V)	-0.33	5	15	80	DPEphos/bq
230(V)	-0.39	0	71	29	bq/DPEphos
229(V)	-0.48	1	17	83	DPEphos/bq
228(V)	-0.53	2	5	93	DPEphos
227(V)	-0.56	3	2	96	DPEphos
226(V)	-0.7	3	3	94	DPEphos
225(V)	-0.79	3	3	94	DPEphos

224(V)	-0.86	2	3	95	DPEphos
223(V)	-1.03	1	1	98	DPEphos
222(V)	-1.15	2	2	96	DPEphos
221(V)	-1.32	1	32	67	DPEphos/bq
220(V)	-1.46	1	66	33	bq/DPEphos
219(V)	-1.69	0	99	1	bq
218(V)	**-2.75**	**2**	**96**	**2**	**bq**
217(O)	**-6.26**	**36**	**7**	**57**	**DPEphos/Cu**
216(O)	-6.75	44	14	42	Cu/DPEphos
215(O)	-6.85	51	31	18	Cu/bq
214(O)	-7.05	11	81	8	bq
213(O)	-7.2	4	28	69	DPEphos/bq
212(O)	-7.27	5	50	45	bq/DPEphos
211(O)	-7.38	0	76	24	bq/DPEphos
210(O)	-7.44	4	2	93	DPEphos
209(O)	-7.5	1	12	86	DPEphos
208(O)	-7.55	0	8	92	DPEphos
207(O)	-7.59	3	7	91	DPEphos
206(O)	-7.63	8	7	85	DPEphos
205(O)	-7.68	3	6	91	DPEphos
204(O)	-7.72	3	1	96	DPEphos
203(O)	-7.78	17	14	69	DPEphos/Cu
202(O)	-7.9	31	6	64	DPEphos/Cu

201(O)	-7.95	41	2	57	DPEphos/Cu
200(O)	-8	69	6	25	Cu/DPEphos
199(O)	-8.04	44	2	53	DPEphos/Cu
198(O)	-8.19	7	8	85	DPEphos
197(O)	-8.3	3	91	6	bq

Tab. A9. Excitation wavelength, oscillator strengths *f* and composition of the first two TD-DFT calculated (G09, [28]; PBE0-GD3 [24-26]) lowest triplet excitations for the ground state of the cations of complexes **1-6** in DCM. H and L denote highest occupied and lowest unoccupied orbitals respectively.

Complex	**State**	**$\lambda_{calc.}$ (nm)**	***f***	**Transition**	**Character**
1	1	463	0.000	H-4->L+1 (44%)	IL
				HOMO->L+1 (18%)	MLCT/LLCT
1	2	437	0.000	HOMO->LUMO (83%)	MLCT/LLCT
2	1	459	0.000	H-4->L+1 (45%)	IL
				HOMO->L+1 (17%)	MLCT/LLCT
2	2	431	0.000	HOMO->LUMO (84%)	MLCT/LLCT
3	1	454	0.000	H-4->L+1 (40%)	IL
				HOMO->L+1 (15%)	MLCT/LLCT
3	2	424	0.000	HOMO->LUMO (85%)	MLCT/LLCT
4	1	462	0.000	H-6->L+1 (19%)	MLCT/LLCT/IL
				H-3->L+1 (19%)	

				HOMO->L+1 (21%)	
4	2	422	0.000	HOMO->LUMO (84%)	MLCT/LLCT
5	1	556	0.000	HOMO->L+1 (87%)	IL
5	2	504	0.000	HOMO->LUMO (94%)	IL
6	1	528	0.000	H-3->LUMO (52%)	MLCT/IL
				H-2->LUMO (17%)	
	2	526		HOMO->LUMO (81%)	MLCT/LLCT

Tab. A10. G09 [28] PBE0-GD3 [24-26] calculated one-electron energy and percentage composition (rounded) of selected frontier MOs expressed in terms of component fragments for the lowest triplet excited state of complex **1** in DCM.

Alpha					
MO	**Energy (eV)**	**Cu**	**phen**	**DPEphos**	**Character**
200(V)	-1.56	2	2	96	DPEphos
199(V)	-1.84	0	99	1	phen
198(O)	-3.68	3	95	3	phen
197(O)	-6.75	13	14	73	DPEphos
196(O)	-7.07	1	90	9	phen
195(O)	-7.28	0	97	3	phen
Beta					
MO	**Energy (eV)**	**Cu**	**phen**	**DPEphos**	**Character**
200(V)	-1.49	1	12	87	DPEphos

199(V)	-1.51	1	85	14	phen
198(V)	-1.8	5	77	18	phen
197(V)	-3.81	52	20	28	Cu/DPEphos/phen
196(O)	-6.74	1	96	3	phen
195(O)	-6.9	1	99	1	phen

Tab. A11. G09 [28] PBE0-GD3 [24-26] calculated one-electron energy and percentage composition (rounded) of selected frontier MOs expressed in terms of component fragments for the lowest triplet excited state of complex **2** in DCM.

Alpha					
MO	**Energy (eV)**	**Cu**	**dmp**	**DPEphos**	**Character**
208(V)	-1.6	1	2	97	DPEphos
207(V)	-1.87	1	96	3	dmp
206(O)	-3.45	2	96	2	dmp
205(O)	-6.56	4	67	29	dmp/DPEphos
204(O)	-6.78	6	38	56	DPEphos/dmp
203(O)	-6.83	1	93	7	dmp
Beta					
MO	**Energy (eV)**	**Cu**	**dmp**	**DPEphos**	**Character**
208(V)	-1.55	1	44	55	DPEphos/dmp
207(V)	-1.59	1	45	54	DPEphos/dmp
206(V)	-1.89	3	90	7	dmp

205(V)	-4.51	56	21	23	Cu/DPEphos/dmp
204(O)	-6.34	2	97	1	dmp
203(O)	-6.52	1	98	1	dmp

Tab. A12. G09 [28] PBE0-GD3 [24-26] calculated one-electron energy and percentage composition (rounded) of selected frontier MOs expressed in terms of component fragments for the lowest triplet excited state of complex **3** in DCM.

Alpha					
MO	**Energy (eV)**	**Cu**	**dbp**	**DPEphos**	**Character**
232(O)	-1.56	2	4	94	DPEphos
231(O)	-1.72	1	94	6	dbp
230(O)	-3.56	2	96	2	dbp
229(O)	-6.83	6	55	39	dbp/DPEphos
228(O)	-7.01	4	60	36	dbp/DPEphos
227(O)	-7.08	2	81	17	dbp
Beta					
MO	**Energy (eV)**	**Cu**	**dbp**	**DPEphos**	**Character**
232(V)	-1.44	0	4	96	DPEphos
231(V)	-1.52	1	10	90	DPEphos
230(V)	-1.71	4	84	12	dbp
229(V)	-4.16	54	19	27	Cu/DPEphos/dbp
228(O)	-6.6	1	97	2	dbp

227(O)	-6.7	0	98	2	dbp

Tab. A13. G09 [28] PBE0-GD3 [24-26] calculated one-electron energy and percentage composition (rounded) of selected frontier MOs expressed in terms of component fragments for the lowest triplet excited state of complex **4** in DCM.

			Alpha		
MO	**Energy (eV)**	**Cu**	**dpep**	**DPEphos**	**Character**
256(V)	-1.51	1	1	97	DPEphos
255(V)	-1.85	0	97	2	dpep
254(O)	-3.7	2	96	2	dpep
253(O)	-6.9	4	70	26	dpep/DPEphos
252(O)	-7.08	3	65	32	dpep/DPEphos
251(O)	-7.16	2	81	18	dpep/DPEphos
			Beta		
MO	**Energy (eV)**	**Cu**	**dpep**	**DPEphos**	**Character**
256(V)	-1.47	1	7	92	DPEphos
255(V)	-1.53	1	83	17	dpep/DPEphos
254(V)	-1.82	4	88	8	dpep
253(V)	-4.28	56	20	24	Cu/DPEphos/dpep
252(O)	-6.64	2	97	1	dpep
251(O)	-6.86	0	98	1	dpep

Tab. A14. G09 [28] PBE0-GD3 [24-26] calculated one-electron energy and percentage composition (rounded) of selected frontier MOs expressed in terms of component fragments for the lowest triplet excited state of complex **5** in DCM.

Alpha					
MO	**Energy (eV)**	**Cu**	**dap**	**DPEphos**	**Character**
208(V)	-1.23	1	1	98	DPEphos
207(V)	-2.04	3	94	3	dap
206(O)	-3.66	0	99	0	dap
205(O)	-6.05	31	24	45	DPEphos/Cu/dap
204(O)	-6.33	9	80	11	dap
203(O)	-6.58	56	23	21	Cu/dap/DPEphos
Beta					
MO	**Energy (eV)**	**Cu**	**dap**	**DPEphos**	**Character**
208(V)	-1.22	1	6	93	DPEphos
207(V)	-1.32	0	93	7	dap
206(V)	-1.7	2	95	3	dap
205(V)	-3.57	0	98	1	dap
204(O)	-6.08	38	7	54	DPEphos/Cu
203(O)	-6.58	56	23	21	Cu/dap/DPEphos

Tab. A15. G09 [28] PBE0-GD3 [24-26] calculated one-electron energy and percentage composition (rounded) of selected frontier MOs expressed in terms of component fragments for the lowest triplet excited state of complex **6** in DCM.

Alpha					
MO	**Energy (eV)**	**Cu**	**bq**	**DPEphos**	**Character**
220(V)	-1.56	2	5	93	DPEphos
219(V)	-1.65	0	90	9	bq
218(O)	-4.2	2	96	2	bq
217(O)	-6.75	5	61	34	bq/DPEphos
216(O)	-6.9	4	67	29	bq/DPEPhos
215(O)	-7.13	1	93	7	bq
Beta					
MO	**Energy (eV)**	**Cu**	**bq**	**DPEphos**	**Character**
220(V)	-1.43	2	1	97	DPEphos
219(V)	-1.53	1	1	97	DPEphos
218(V)	-2.41	4	92	5	bq
217(V)	-4.13	53	21	26	Cu/DPEphos/bq
216(O)	-6.48	1	96	3	bq
215(O)	-6.85	3	90	7	bq

Figures

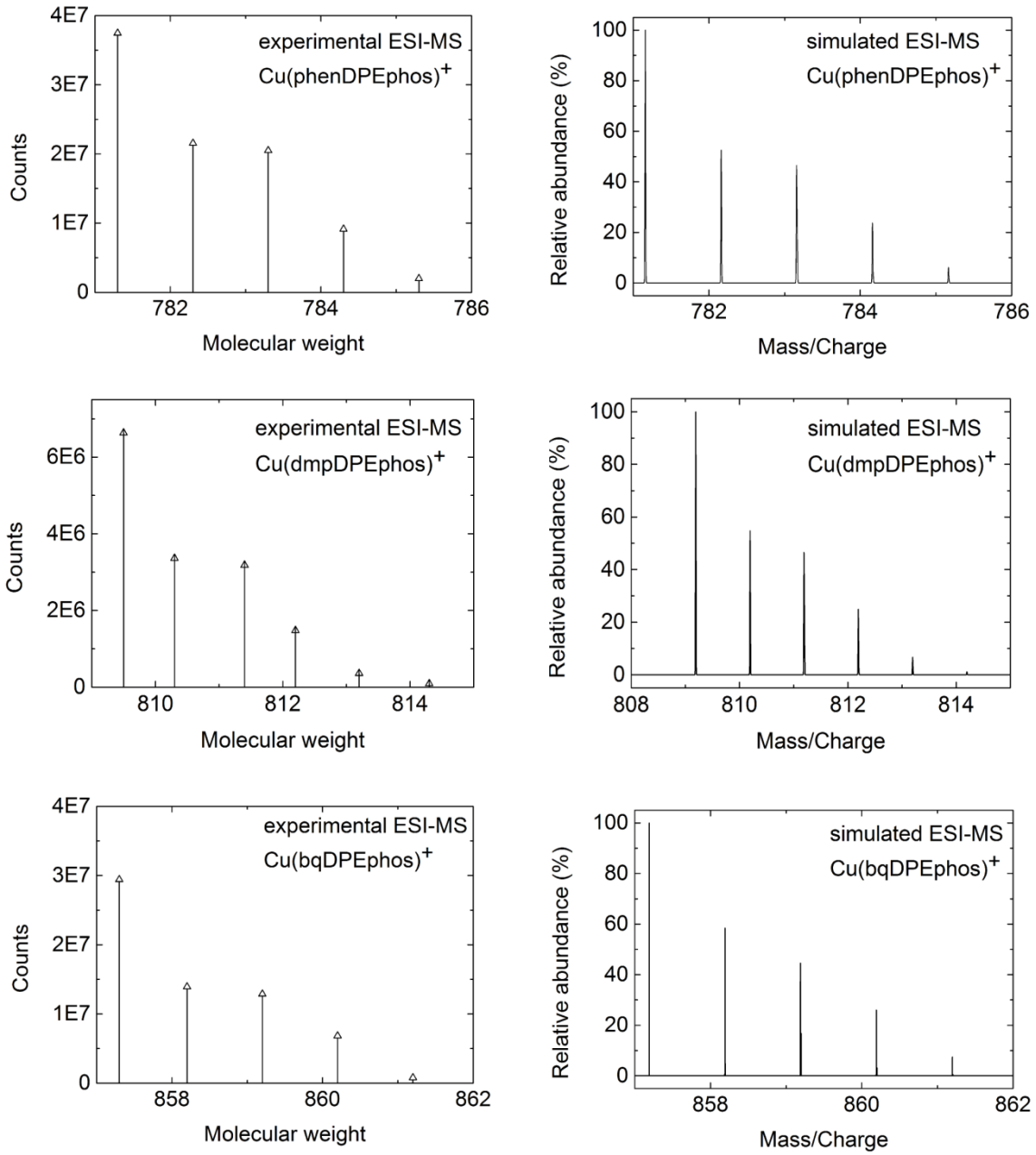

Fig. A1. Experimental (**left**) and simulated (**right**) electrospray ionization mass spectra (ESI-MS) of complex **1** (**top**), complex **2** (**middle**) and **6** (**bottom**).

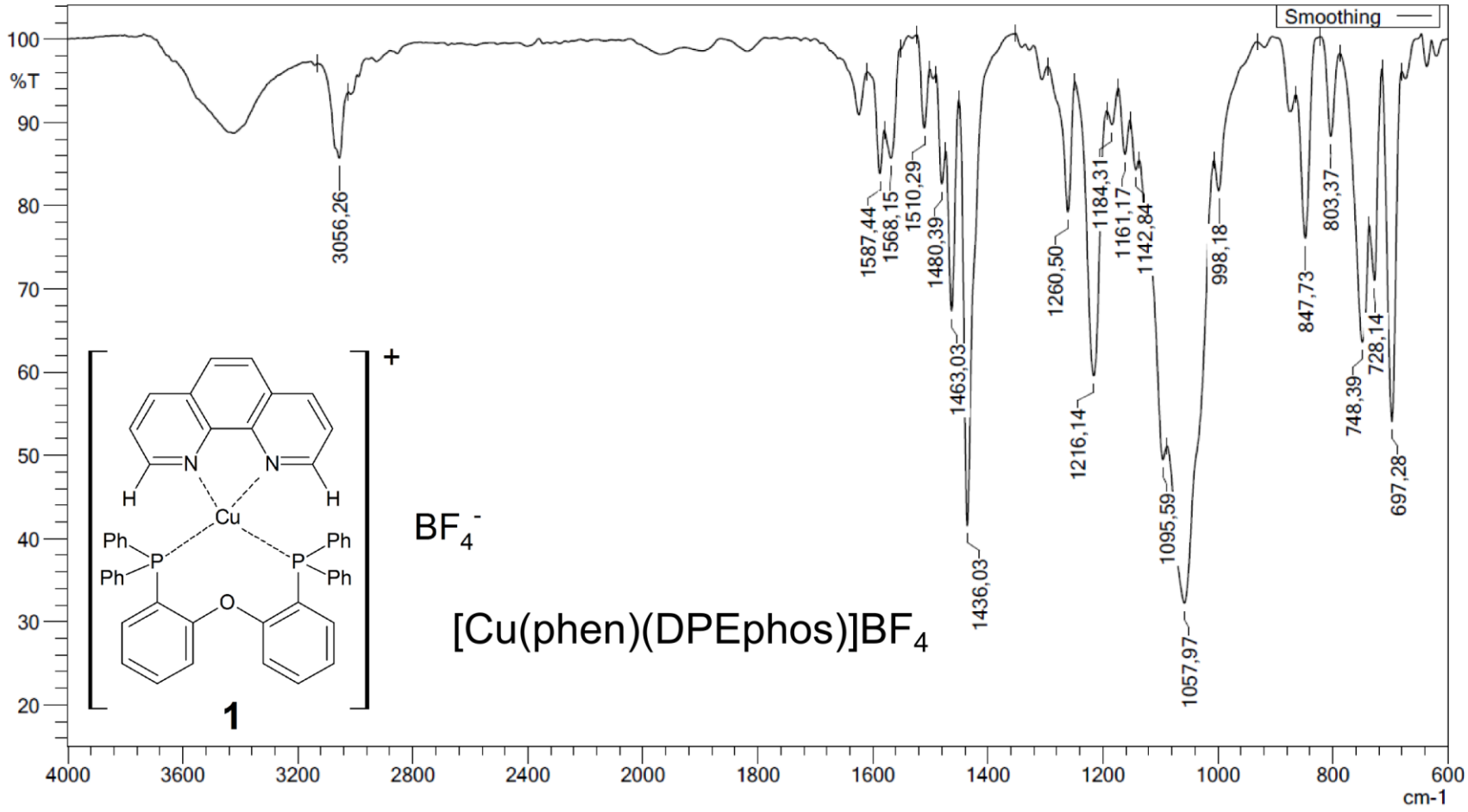

Fig. A2. The FT-IR spectrum of complex **1** in KBr pellets.

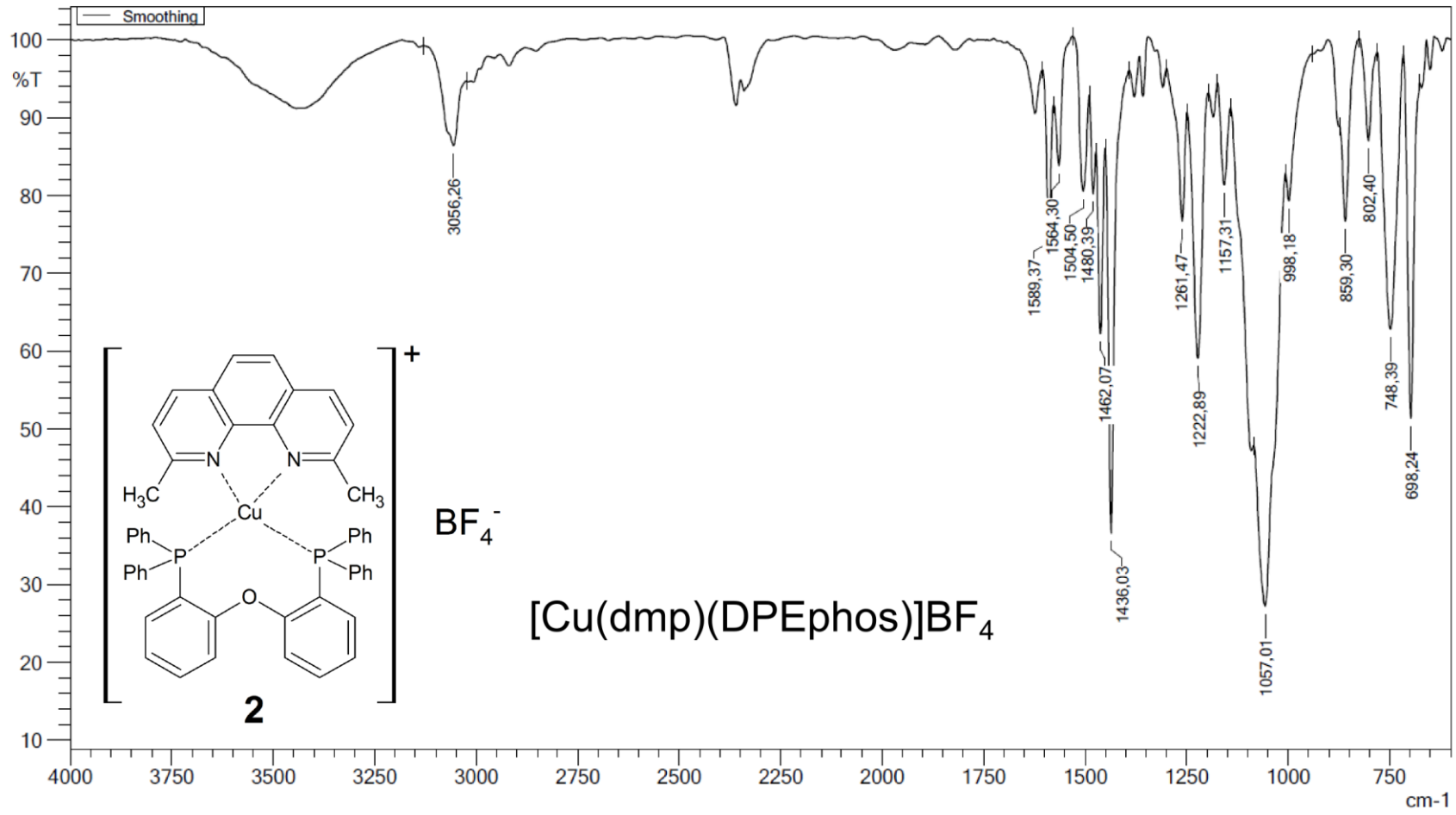

Fig. A3. The FT-IR spectrum of complex **2** in KBr pellets.

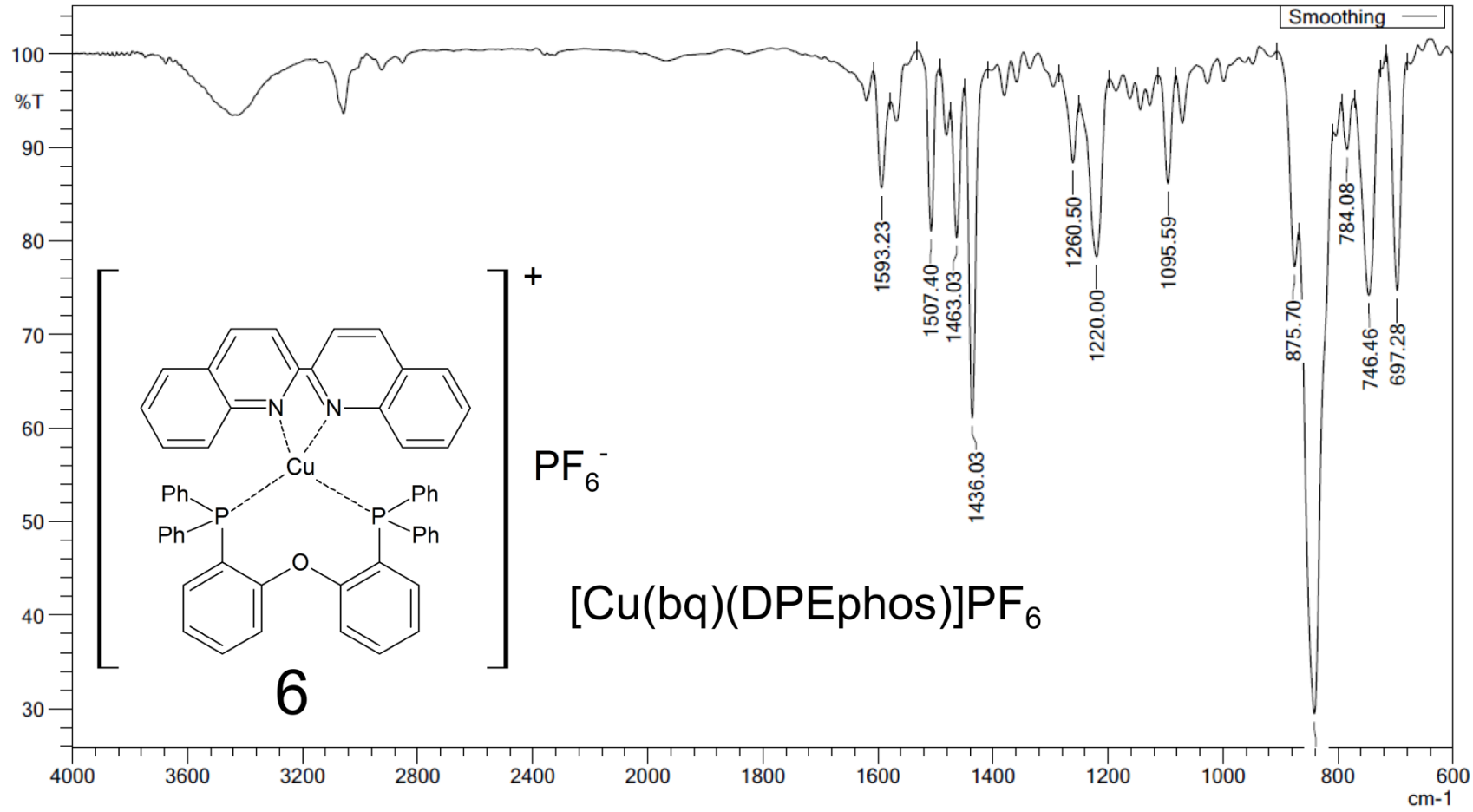

Fig. A4. The FT-IR spectrum of complex **6** in KBr pellets.

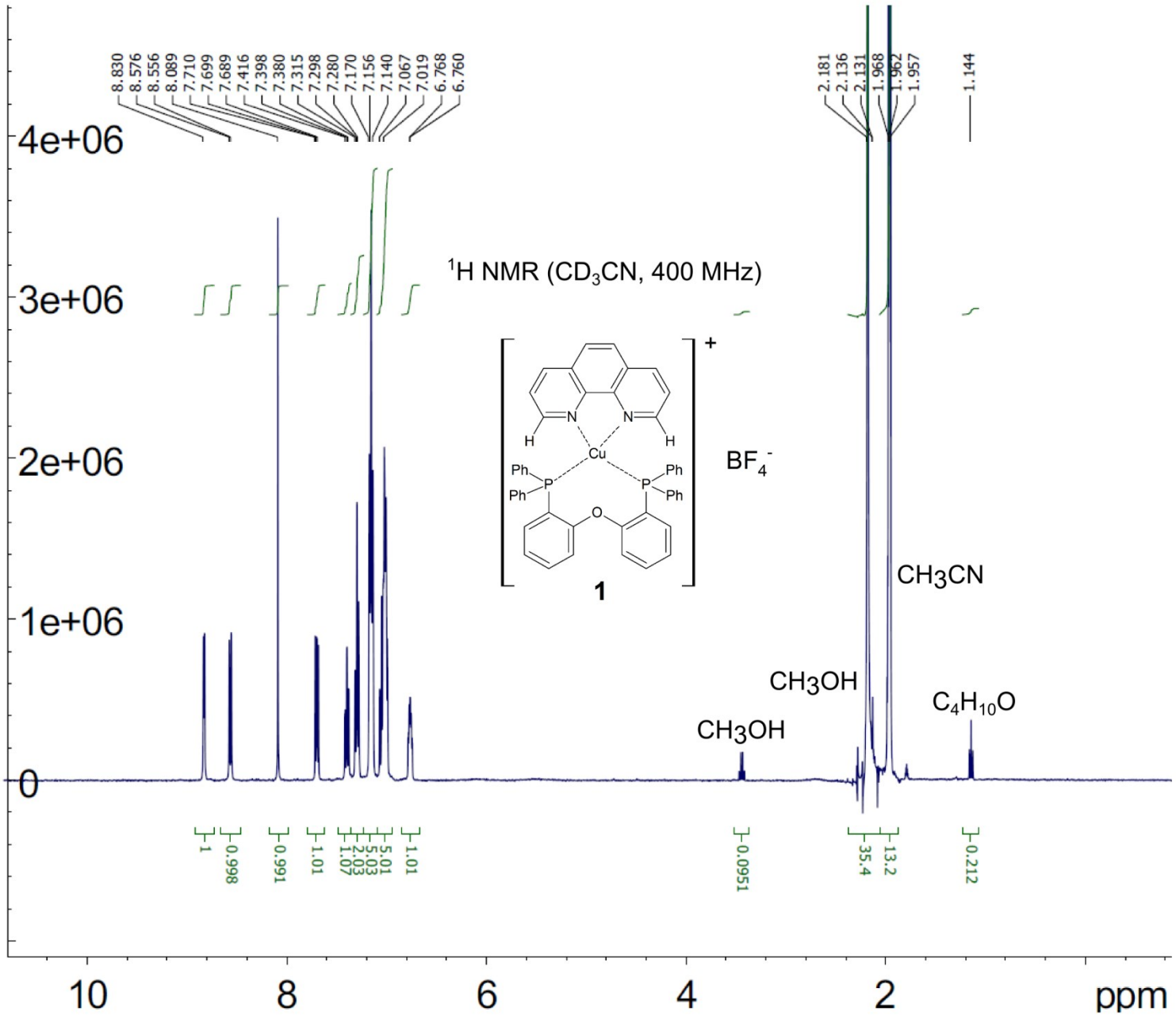
8.830
8.576
8.556
8.089
7.710
7.699
7.689
7.416
7.398
7.380
7.315
7.298
7.280
7.170
7.156
7.140
7.067
7.019
6.768
6.760
2.181
2.136
2.131
1.968
1.962
1.957
1.144
4e+06
3e+06
2e+06
1e+06
0
^{1}H NMR (CD_3CN, 400 MHz)
BF_4^-
1
CH_3CN
CH_3OH
CH_3OH
$C_4H_{10}O$
1
0.998
0.991
1.01
1.07
2.03
5.01
1.01
0.0951
35.4
13.2
0.212
10
8
6
4
2
ppm

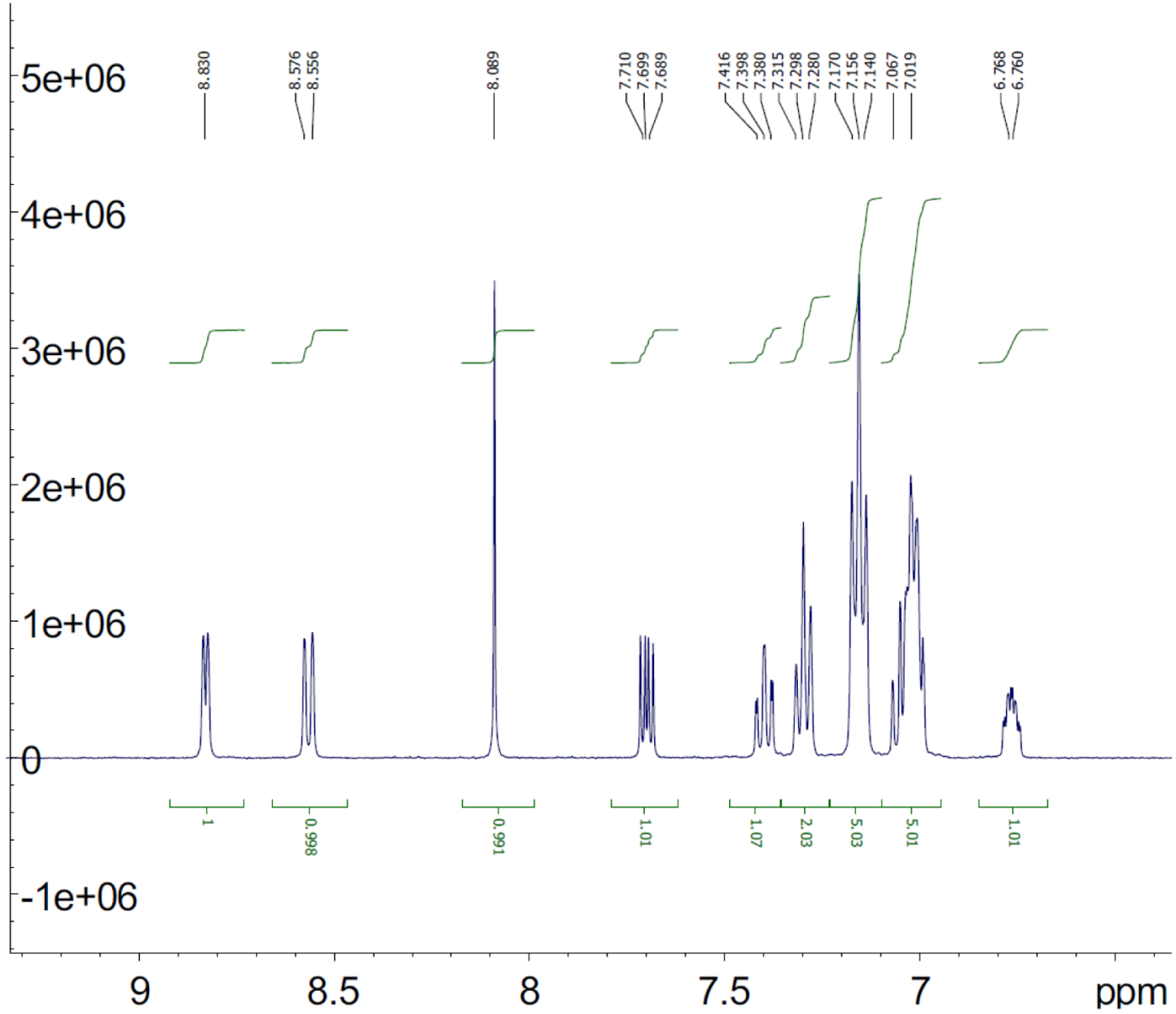

Fig. A5. ^{1}H-NMR spectrum of complex **1** in CD_3CN. Full spectrum (**page 40**) and spectrum between 6.5-9.5 ppm (**page 41**).

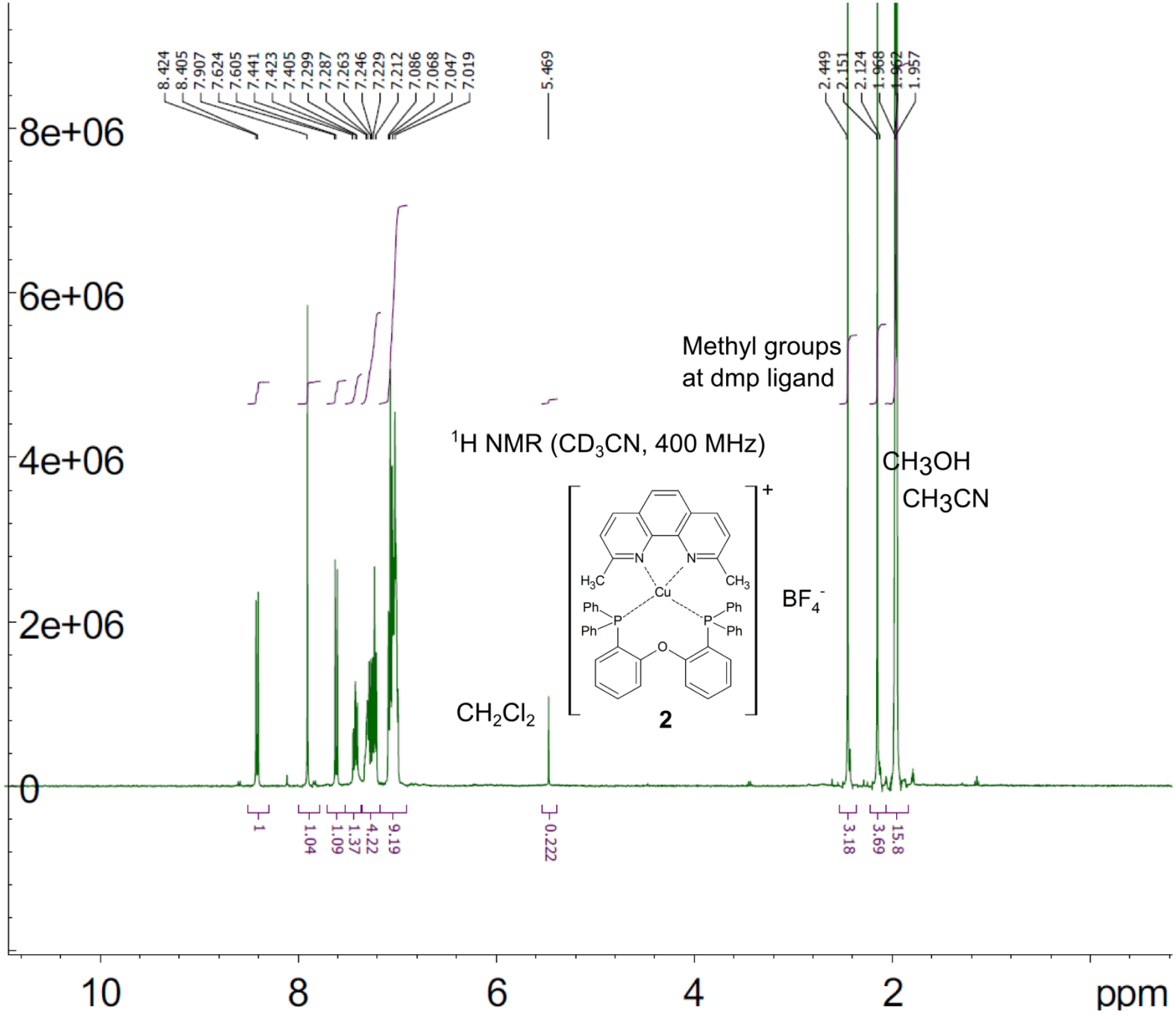
8.424
8.405
7.907
7.624
7.605
7.441
7.423
7.405
7.299
7.287
7.263
7.246
7.229
7.212
7.086
7.068
7.047
7.019
5.469
2.449
2.151
2.124
1.968
1.962
1.957
8e+06
6e+06
4e+06
2e+06
0
Methyl groups
at dmp ligand
^{1}H NMR (CD_3CN, 400 MHz)
CH_3OH
CH_3CN
CH_2Cl_2
BF_4^-
2
1
1.04
1.09
1.37
4.22
9.19
0.222
3.18
3.69
15.8
10
8
6
4
2
ppm

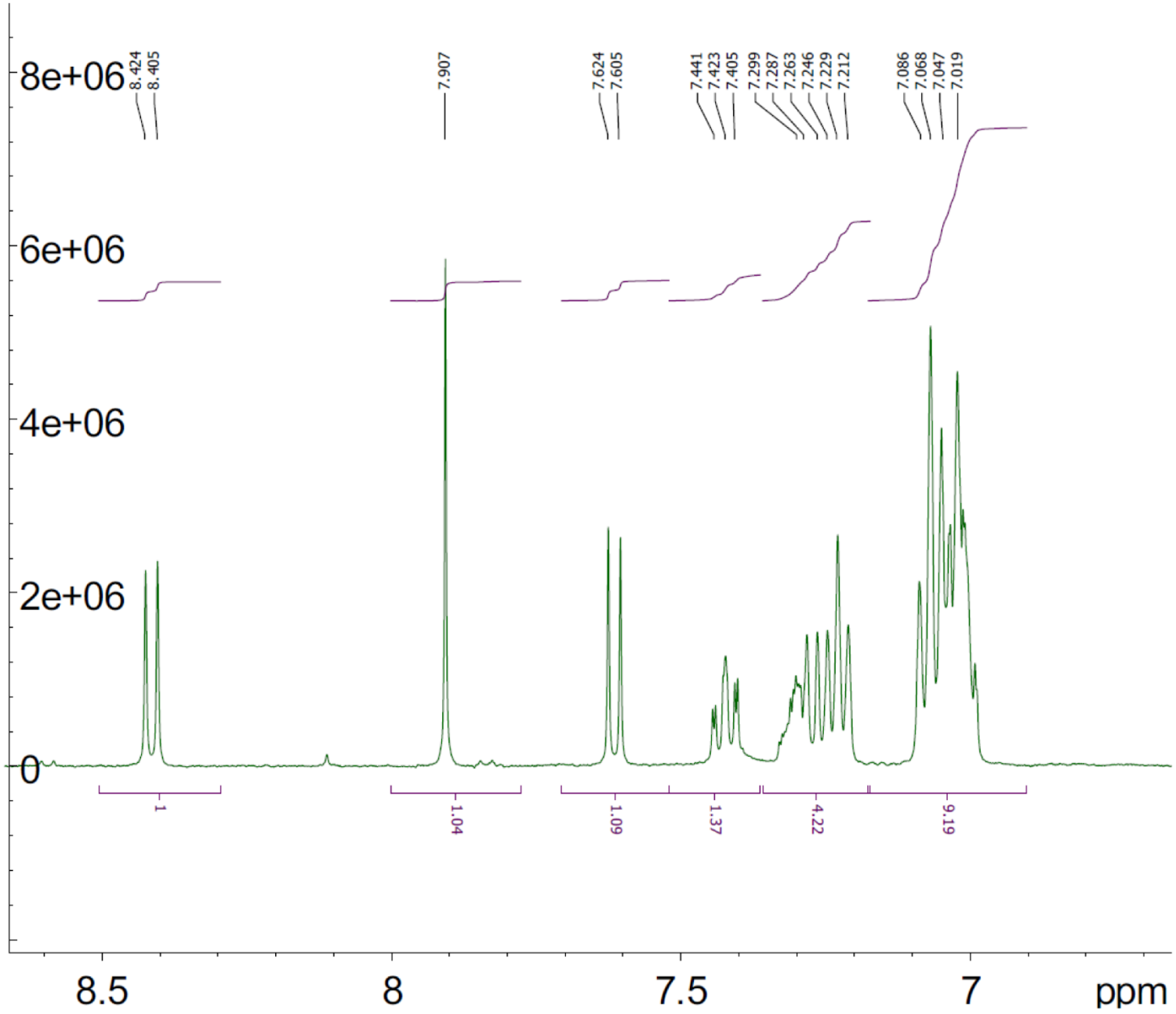

Fig. A6. ^{1}H-NMR spectrum of complex **2** in CD_3CN. Full spectrum (**page 42**) and spectrum between 6.5-8.5 ppm (**page 43**).

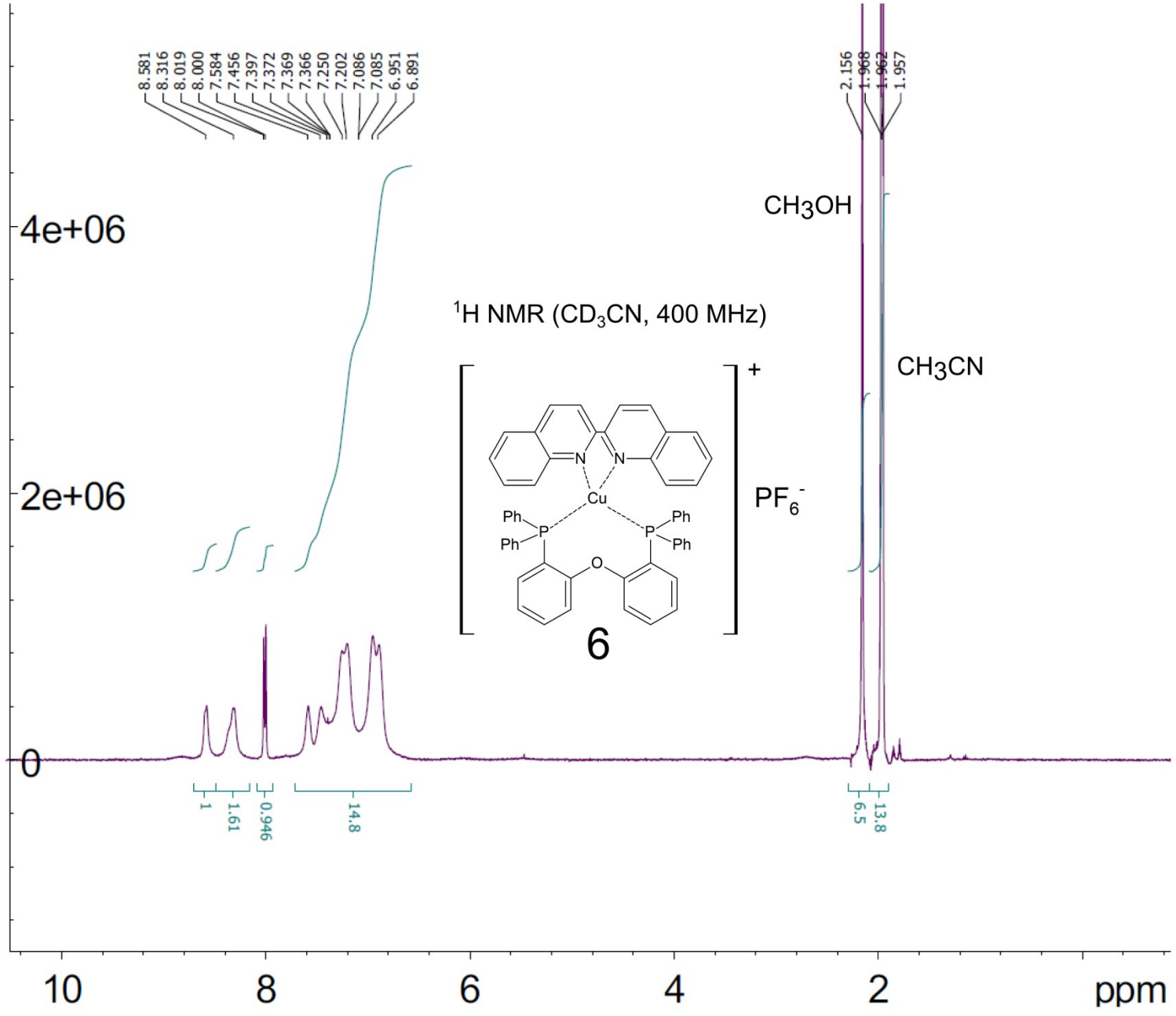
8.581
8.316
8.019
8.000
7.584
7.456
7.397
7.372
7.369
7.366
7.250
7.202
7.086
7.085
6.951
6.891
2.156
1.968
1.962
1.957
CH3OH
CH3CN
4e+06
2e+06
0
1H NMR (CD3CN, 400 MHz)
PF6-
6
1
1.61
0.946
14.8
6.5
13.8
10
8
6
4
2
ppm

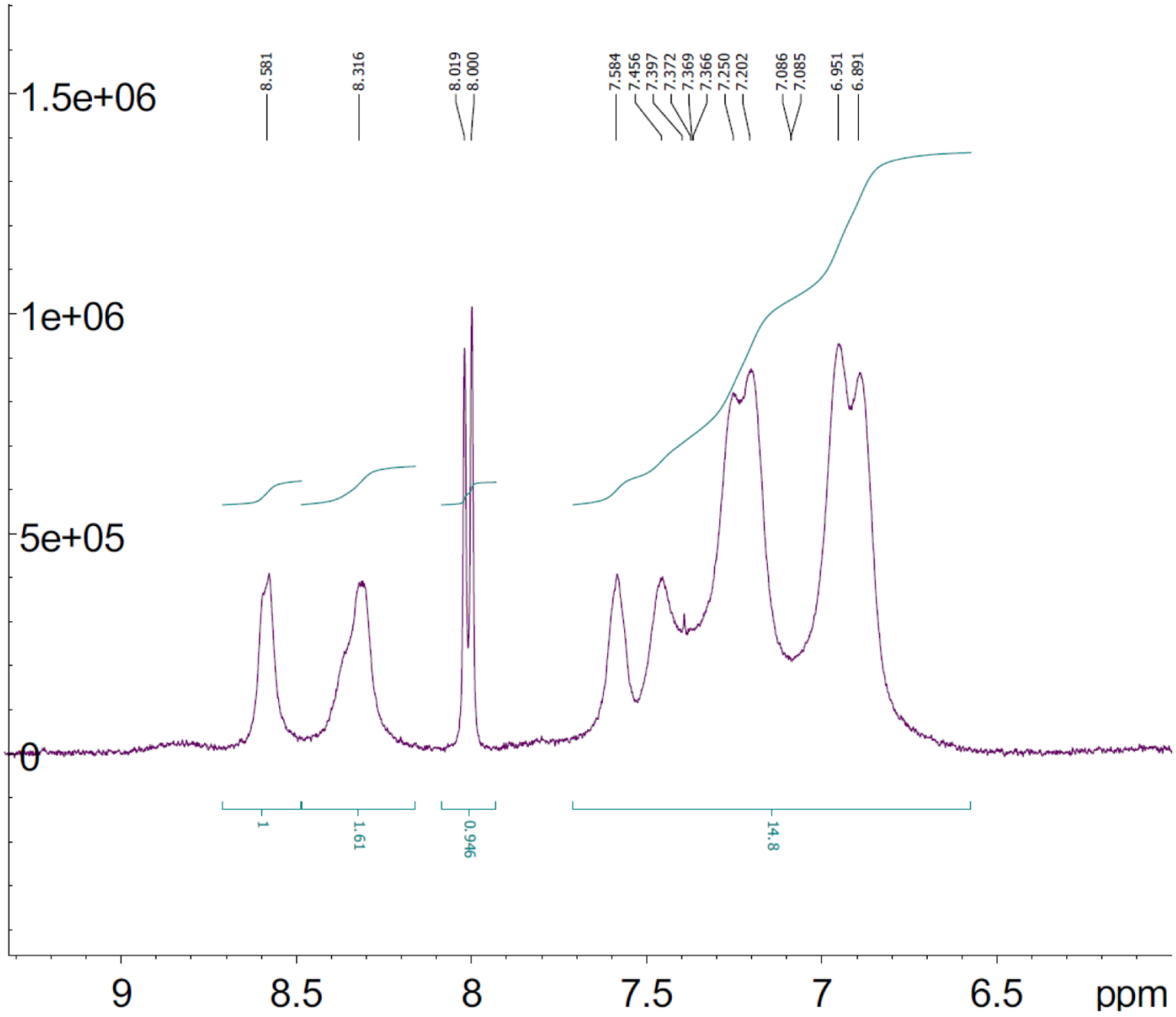

Fig. A7. ^{1}H-NMR spectrum of complex **6** in CD_3CN. Full spectrum (**page 44**) and spectrum between 6.5-9.0 ppm (**page 45)**.

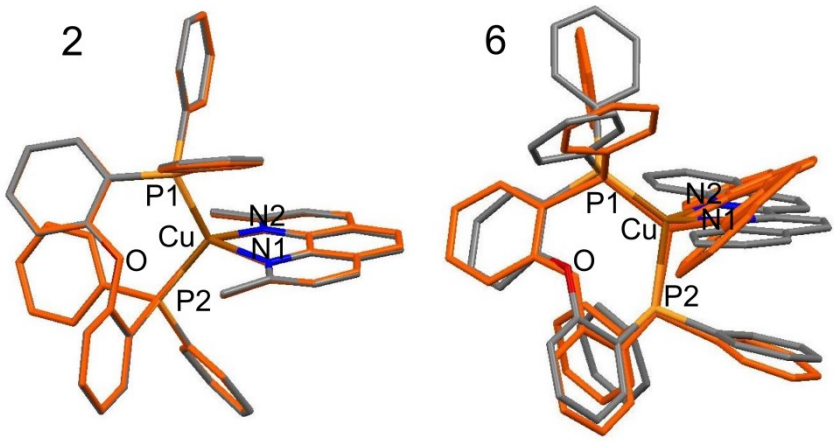

Fig. A8. (**Left**) Superposition of the molecular structure of complex **2** determined by crystallography within this work (orange) and by Kuang et al. (element-colored) [2]. (**Right**) Superposition of the molecular structure of complex **6** determined by crystallography within this work (orange) and by Zhang et al. (element-colored) [5].

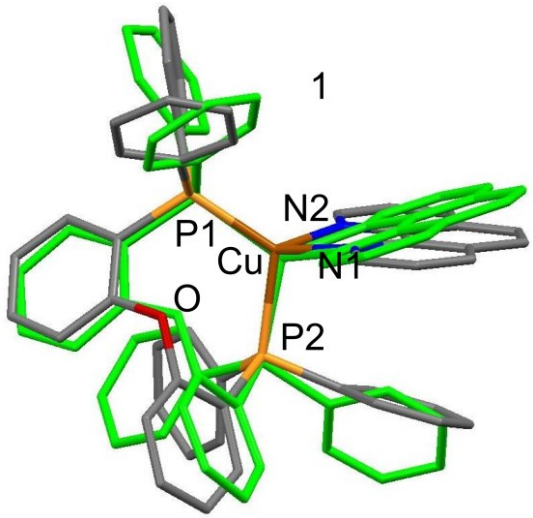

Fig. A9. Superposition of the PBE0-GD3-optimized [24-26] molecular structure (green) (G09 [28]) of complex **1** in its ground state and the XRD structure (element-colored) as determined in this work.

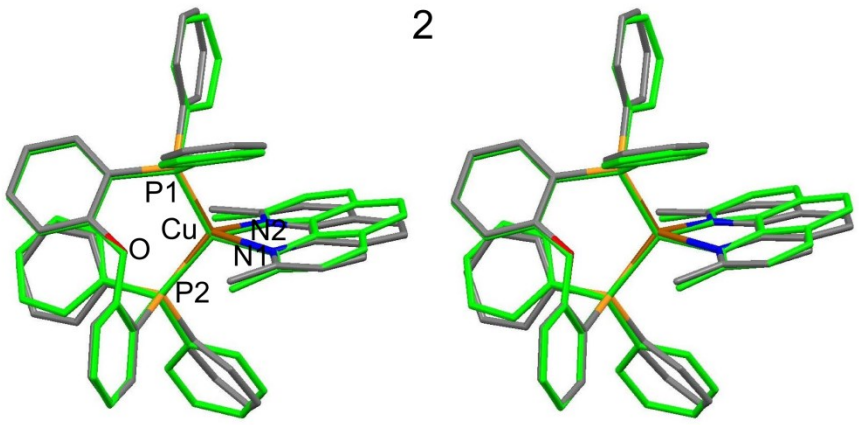

Fig. A10. Superposition of the PBE0-GD3-optimized [24-26] molecular structure (green) (G09 [28]) of complex **2** in its ground state and the XRD structure (element-colored) as determined by Kuang et al [2] (**left**) and in this work (**right**).

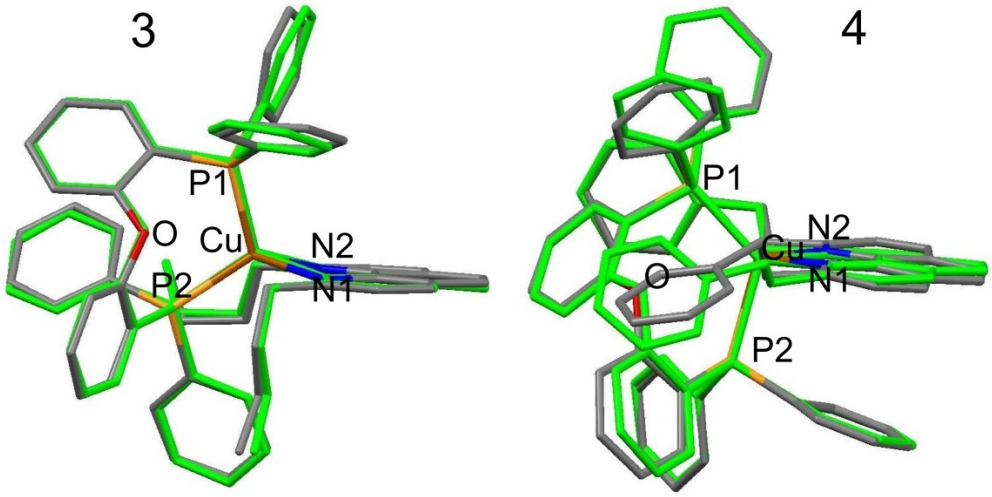

Fig. A11. Superposition of the PBE0-GD3-optimized [24-26] molecular structure (green) (G09 [28]) of complex **3** (**left**) and **4** (**right**) in their ground states and the XRD structure (element-colored) as determined by Kuang et al. [2] and Armaroli et al.[14] respectively.

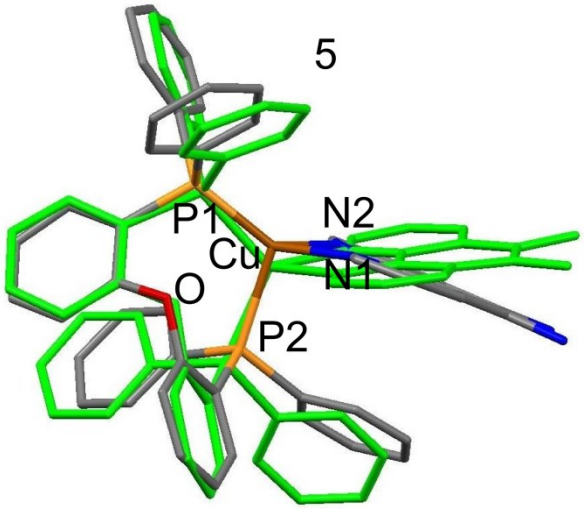

Fig. A12. Superposition of the PBE0-GD-optimized [24-26] molecular structure (green) (G09 [28]) of complex **5** in its ground state and the XRD structure (element-colored) as determined by Yao et al. [15].

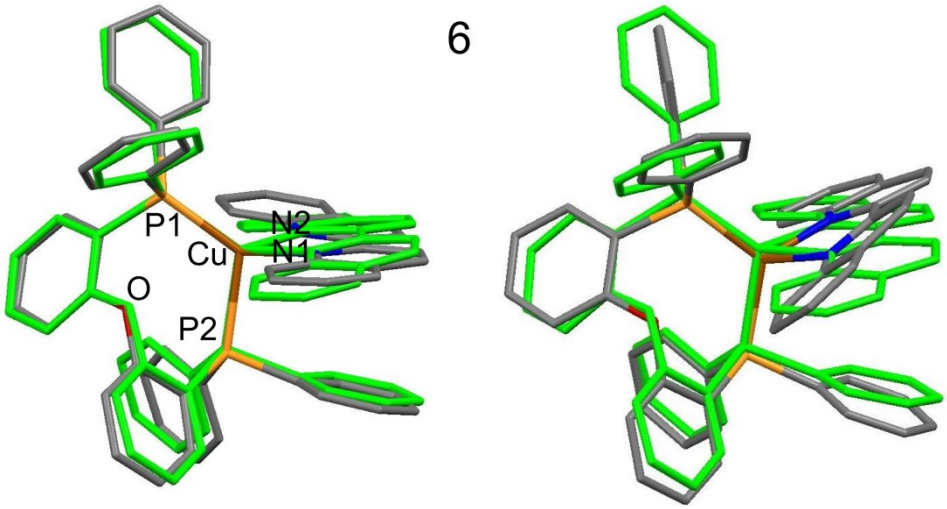

Fig. A13. Superposition of the PBE0-GD3-optimized [24-26] molecular structure (green) (G09 [28]) of complex **6** in its ground state and the XRD structure (element-colored) as determined by Kuang et al. [2] (**left**) and in this work (**right**).

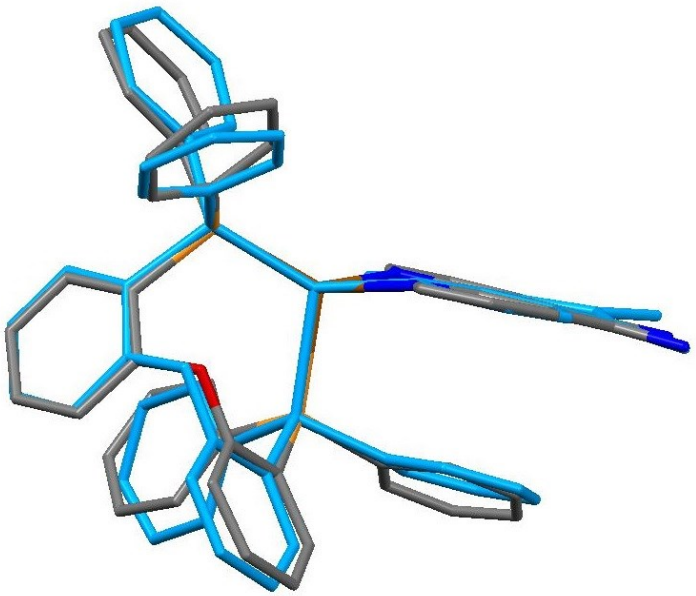

Fig. A14. Superposition of the PBE0-GD-optimized [24-26] molecular structure of complex **5** in the lowest triplet excited state (blue) (G09 [28]) and the XRD structure (element-colored) as determined by Yao et al. [15].

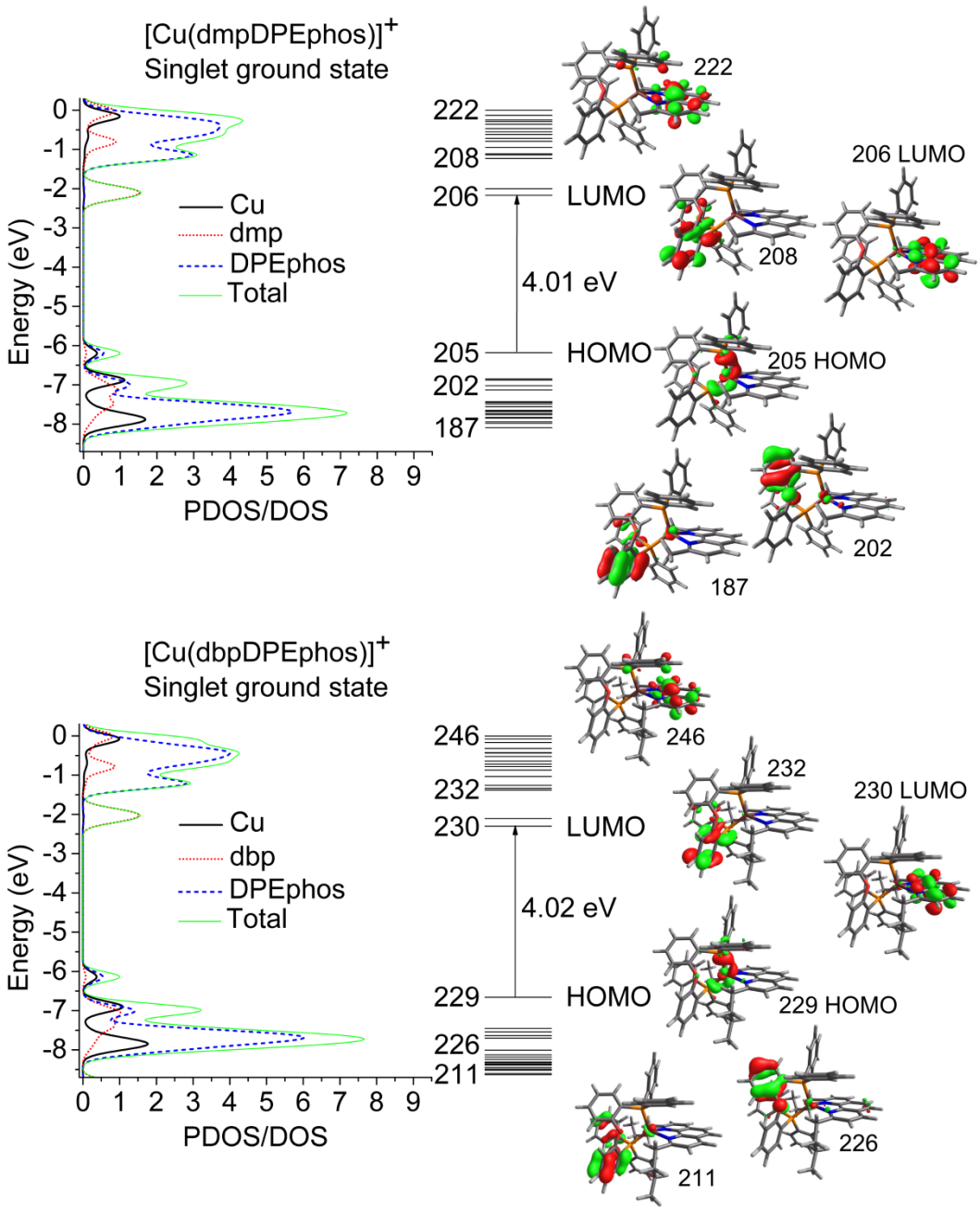

Figure A15. Total and partial density of states (DOS/PDOS) and energy-level diagram of the frontier molecular orbitals together with selected three-dimensional MO plots calculated by DFT using G09 [28] at the PBE0-GD3 [24-26] level for the ground state of complex **2** (**top**) and **3** (**bottom**) in the DCM. For clarity, only a few of the molecular orbitals are numbered.

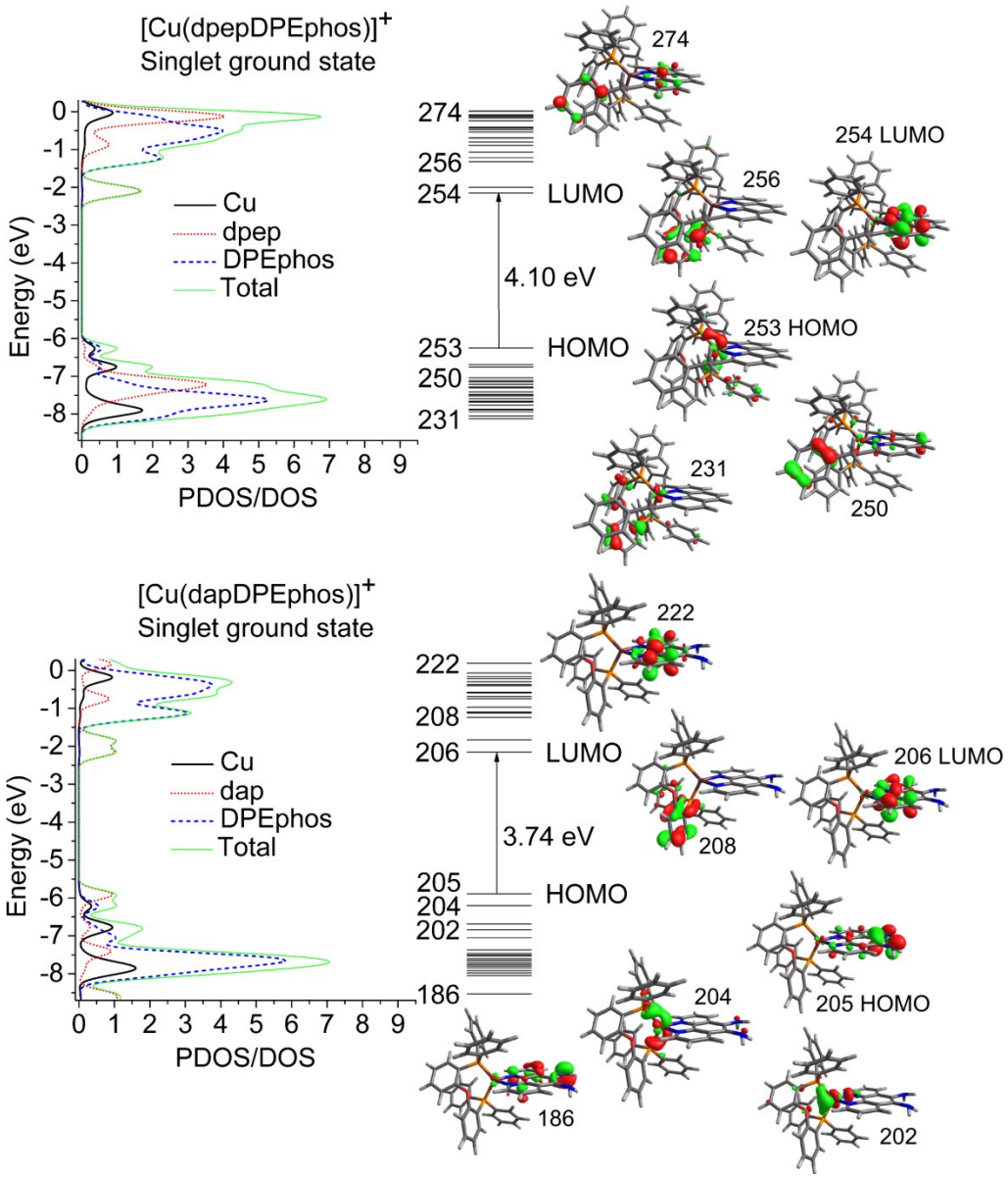

Figure A16. Total and partial density of states (DOS/PDOS) and energy-level diagram of the frontier molecular orbitals together with selected three-dimensional MO plots calculated by DFT using G09 [28] at the PBE0-GD3 [24-26] level for the ground state of complex **4** (**top**) and **5** (**bottom**) in the DCM. For clarity, only a few of the molecular orbitals are numbered.

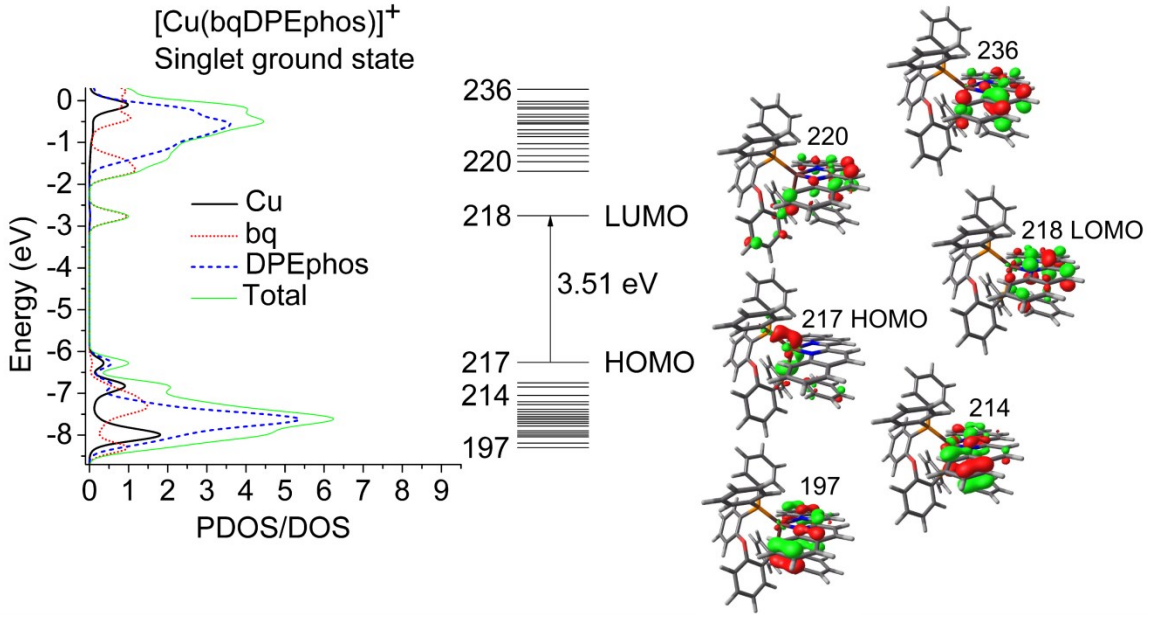

Fig. A17. Total and partial density of states (DOS/PDOS) and energy-level diagram of the frontier molecular orbitals together with selected three-dimensional MO plots calculated by DFT using G09 [28] at the PBE0-GD3 [24-26] level for the ground state of complex **6** in the DCM. For clarity, only a few of the molecular orbitals are numbered.

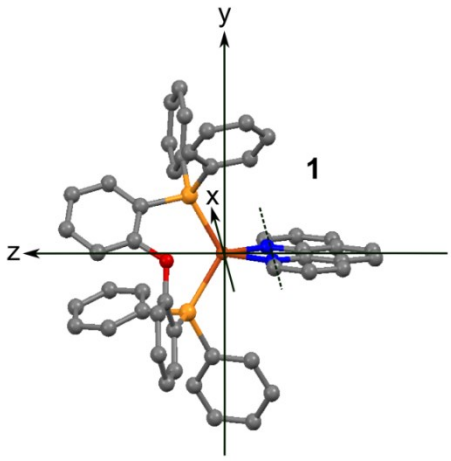

Fig. A18. Complex **1**: Definition of the coordinate system for naming of molecular orbitals.

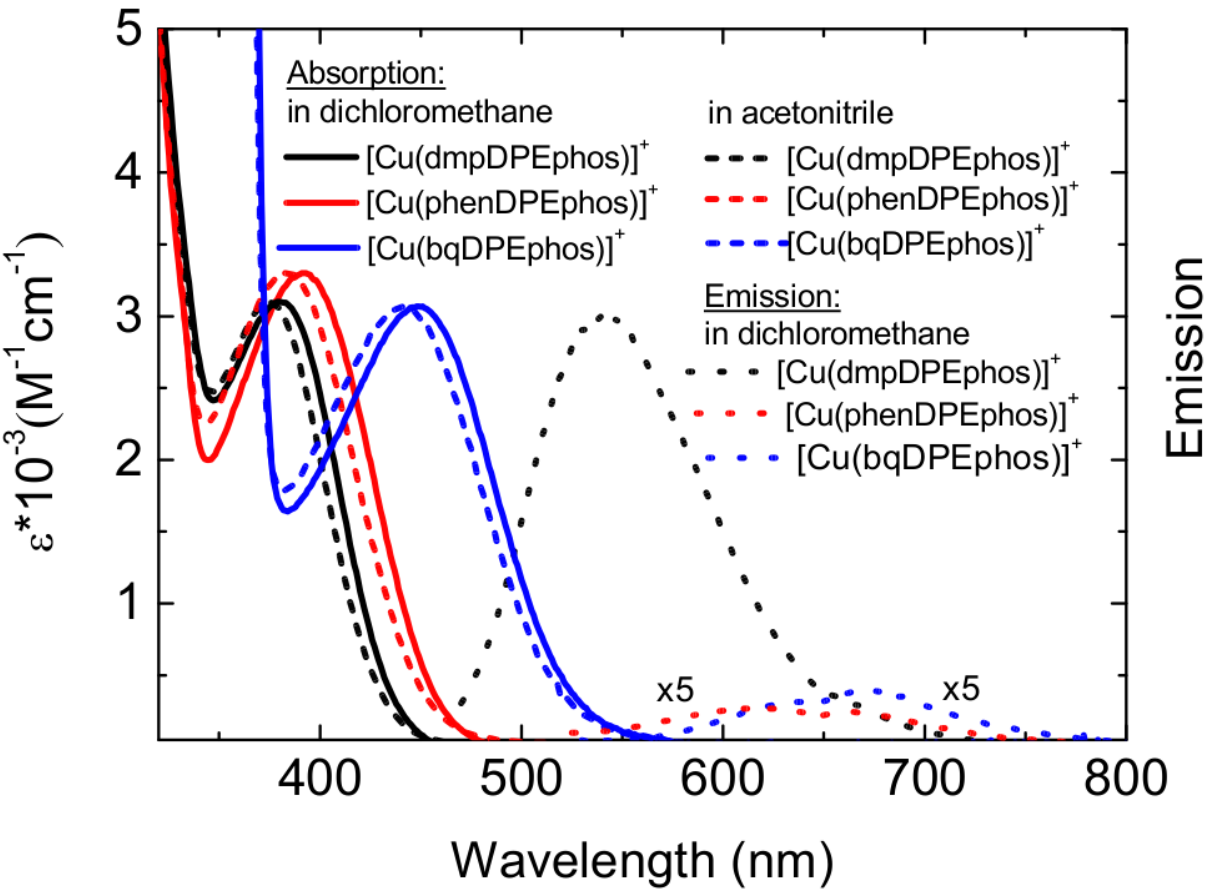

Fig. A19. Absorption and emission spectra in solution at room temperature. Absorbance (left axis) of complex **2** $[Cu(dmp)(DPEphos)]^+$ in DCM (black solid line) and ACN (black dashed line), complex **1** $[Cu(phen)(DPEphos)]^+$ in DCM (red solid line) and ACN (red dashed line), and complex **6** $[Cu(bq)(DPEphos)]^+$ in DCM (blue solid line) and ACN (blue dashed line). Emission spectra (right axis, a.u.) of complex **2** $[Cu(dmp)(DPEphos)]^+$ (black dotted line), complex **1** $[Cu(phen)(DPEphos)]^+$ (red dotted line) and complex **6** $[Cu(bq)(DPEphos)]^+$ (blue dotted line). For better visualization emission spectra for complex **1** and **6** are multiplied by a factor of 5. Extinction coefficients were determined from concentration-dependent absorption measurements.

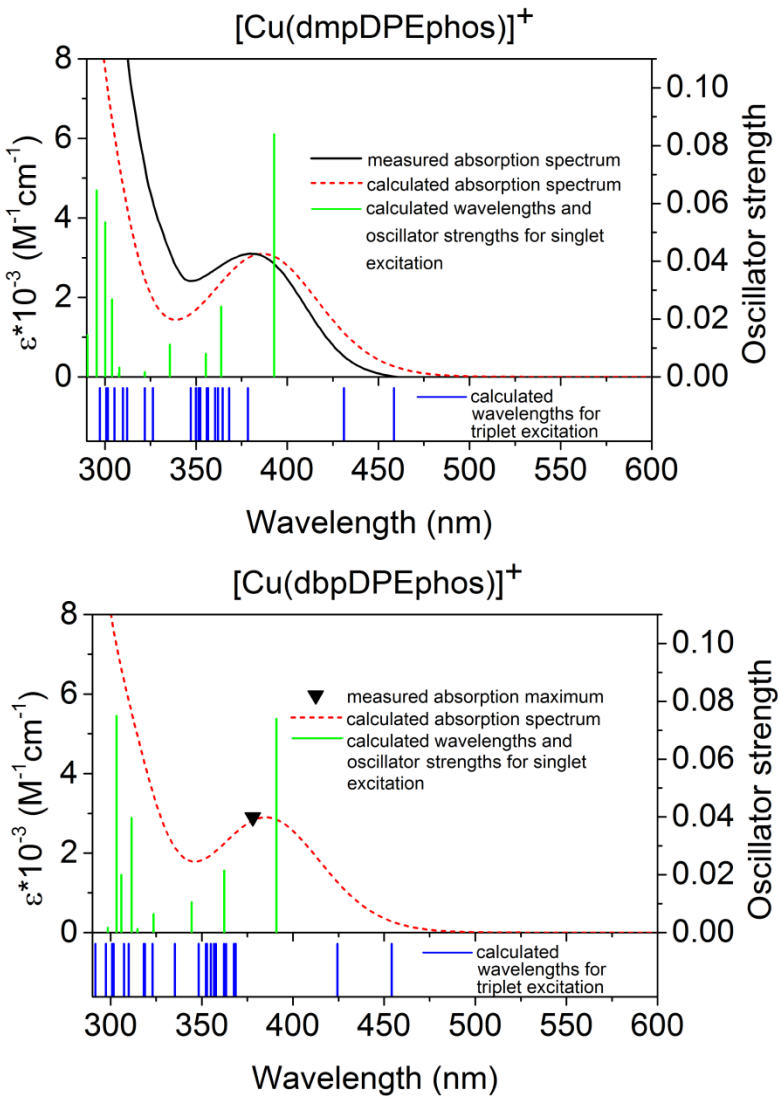

Fig. A20. Experimentally measured (black solid line or black triangle [2]), and TD-DFT calculated (G09, [28]; PBE0-GD3 [24-26]) (red dashed line) absorption spectrum (lines) or band maximum (triangle), transition wavelengths and oscillator strengths for singlet excitation (green lines) and for triplet excitation (blue lines) of the ground state of complex **2** (**top**) and complex **3** (**bottom**) in DCM. To obtain the theoretical absorption spectrum TD-DFT transition lines were convoluted with Gaussians of FWHM 4000/cm using Gaussum 2.2. [10] and calculated extinction coefficients were scaled to match experimental values.

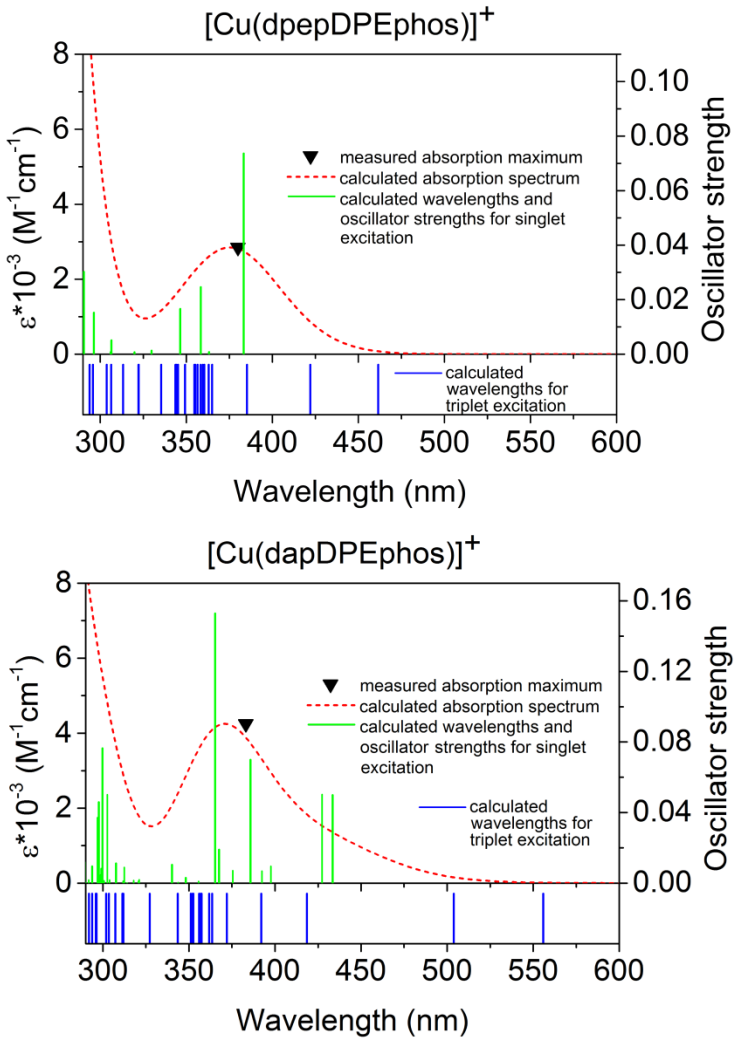

Fig. A21. Experimentally measured (black triangles; data from Refs. [14] (4) and [15] (5)) and TD-DFT calculated (G09, [28]; PBE0-GD3 [24-26]) (red dashed line) absorption spectrum (lines) or band maximum (triangle), transition wavelengths and oscillator strengths for singlet excitation (green lines) and for triplet excitation (blue lines) of the ground state of complex **4** (**top**) and complex **5** (**bottom**) in DCM. To obtain the theoretical absorption spectrum TD-DFT transition lines were convoluted with Gaussians of FWHM 4000/cm using Gaussum 2.2. [10] and calculated extinction coefficients were scaled to match experimental values.

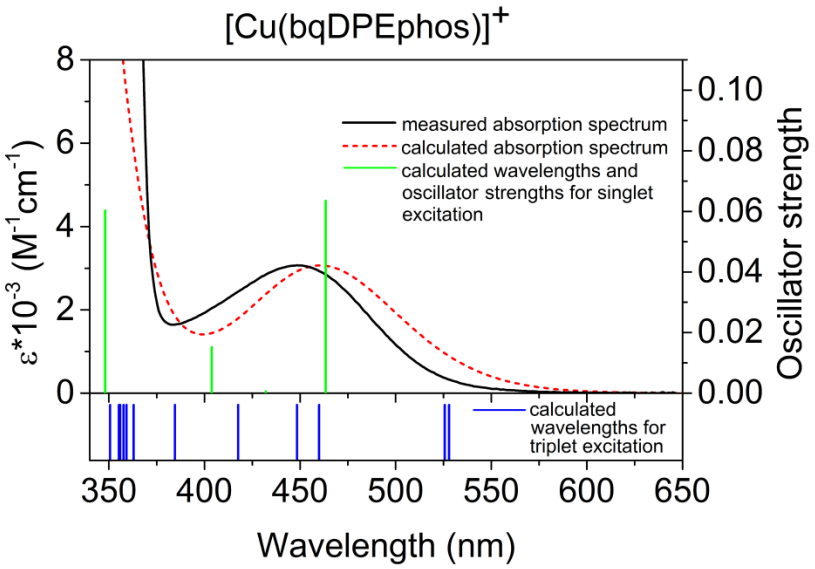

Fig. A22. Experimentally measured (black solid line) and TD-DFT calculated (G09, [28]; PBE0-GD3 [24-26]) absorption spectrum (red dashed line), transition wavelengths and oscillator strengths for singlet excitation (green lines) and for triplet excitation (blue lines) of the ground state of complex **6** in DCM. To obtain the theoretical absorption spectrum TD-DFT transition lines were convoluted with Gaussians of FWHM 4000/cm using Gaussum 2.2. [10] and calculated extinction coefficients were scaled to match experimental values.

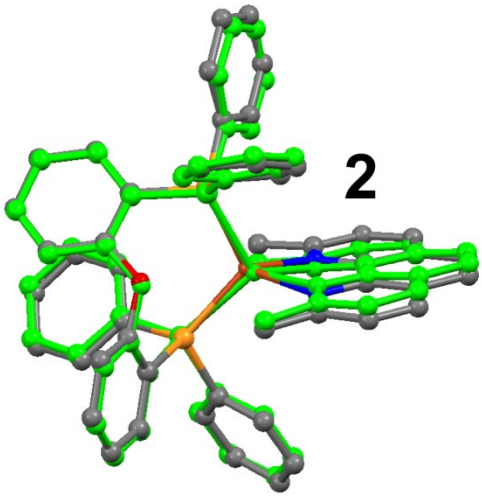

Fig. A23. Comparison of the molecular structure of complex **2** in DCM in its lowest lying triplet (element-colored) and singlet excited state after geometric relaxation (green) as calculated with a DFT/TD-DFT approach using G09 [28].